
(De-)Randomized Smoothing for Decision Stump Ensembles

Miklós Z. Horváth*, Mark Niklas Müller*, Marc Fischer, Martin Vechev

Department of Computer Science

ETH Zurich, Switzerland

mihorvat@ethz.ch, {mark.mueller, marc.fischer, martin.vechev}@inf.ethz.ch

Abstract

Tree-based models are used in many high-stakes application domains such as finance and medicine, where robustness and interpretability are of utmost importance. Yet, methods for improving and certifying their robustness are severely under-explored, in contrast to those focusing on neural networks. Targeting this important challenge, we propose deterministic smoothing for decision stump ensembles. Whereas most prior work on randomized smoothing focuses on evaluating arbitrary base models approximately under input randomization, the key insight of our work is that decision stump ensembles enable exact yet efficient evaluation via dynamic programming. Importantly, we obtain deterministic robustness certificates, even jointly over numerical and categorical features, a setting ubiquitous in the real world. Further, we derive an MLE-optimal training method for smoothed decision stumps under randomization and propose two boosting approaches to improve their provable robustness. An extensive experimental evaluation shows that our approach yields significantly higher certified accuracies than the state-of-the-art for tree-based models. We release all code and trained models at ANONYMIZED.

1 Introduction

Tree-based models have long been a favourite for making decisions in high-stakes domains such as medicine and finance, due to their interpretability and exceptional performance on structured data [1]. However, recent results have highlighted that tree-based models are, similarly to other machine learning models [2, 3], also highly susceptible to adversarial examples [4–6], raising concerns about their use in high-stakes domains where errors can have dire consequences.

While the robustness of neural models has received considerable attention [7–21], the challenge of obtaining robustness guarantees for ensembles of tree-based models has only been investigated recently [4, 22, 23]. However, these initial works only consider numerical features and are based on worst-case approximations, which do not scale well to the difficult ℓ_p -norm setting.

This Work In this work, we address this challenge and present DRS, a novel **DeRandomized Smoothing** approach, for constructing robust tree-based models with deterministic ℓ_p -norm guarantees while supporting both categorical *and* numerical variables. Unlike prior work, our method is based on Randomized Smoothing (RS) [24], an approach that obtains robustness guarantees by evaluating a general base model under an input randomization $\phi(\mathbf{x})$. However, in contrast to standard applications of RS, which use costly and imprecise approximations via sampling and only obtain probabilistic certificates, we leverage the structure of decision stump ensembles to compute their exact output distributions for a given input randomization scheme and thus obtain deterministic certificates. Our key insight is that this distribution can be efficiently computed by aggregating independent distributions associated with the individual features used by the ensemble.

*Equal contribution

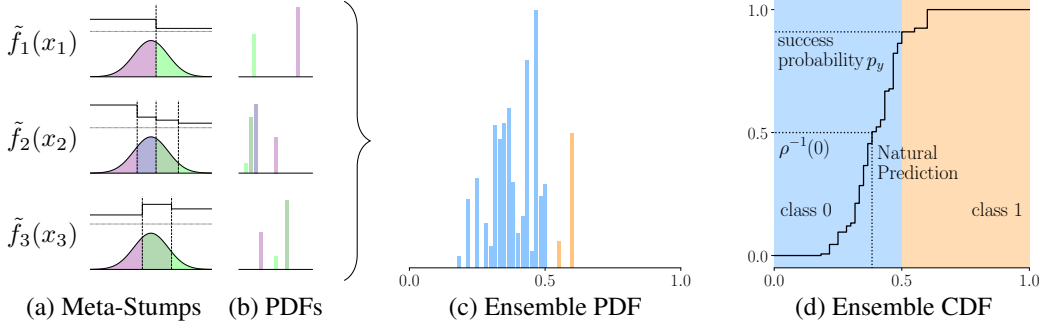


Figure 1: Given an ensemble of 3 meta-stumps \tilde{f}_i (piecewise constant univariate functions), each operating on a different feature x_i of an input \mathbf{x} , we calculate the probability of every output under input randomization (a) to obtain a distribution over their outputs (b). We aggregate these individual PDFs via dynamic programming to obtain the probability distribution over the ensemble’s outputs (c). We can then compute the corresponding CDF (d) to evaluate the smoothed stump ensemble exactly.

We illustrate this idea in Fig. 1: In (a), we show an ensemble of decision stumps over three features (x_1, x_2, x_3) , aggregated to piecewise constant functions over one feature each (discussed in Section 3) and evaluated under the input randomization $\phi(\mathbf{x})$, here a Gaussian. We can compute the independent probability density functions of their outputs (PDFs) (shown in (b)) directly, by evaluating the (Gaussian) cumulative density function (CDF) over the constant regions. Aggregating the individual PDFs (discussed in Section 3), we can efficiently compute the exact PDF (c) and CDF (d) of the ensemble’s output. To evaluate and certify the smoothed model, we can now simply look up the median prediction and success probability, respectively, in the CDF, without requiring sampling.

DRS combines ℓ_p -norm certificates over numerical features, computed as described above, with an efficient worst-case analysis for ℓ_0 -perturbations of categorical features in order to, for the first time, provide joint certificates. To train models amenable to certification with DRS, we propose a robust MLE optimality criterion for training individual stumps and two boosting schemes targeting the certified robustness of the whole ensemble. We show empirically that DRS significantly improves on the state-of-the-art, increasing certified accuracies on established benchmarks up to 4-fold.

Main Contributions Our key contributions are:

- DRS, a novel and efficient Derandomized Smoothing approach for robustness certification, enabling joint deterministic certificates over numerical and categorical variables (Section 3).
- A novel MLE optimality criterion for training decision stumps robust under input randomization and two boosting approaches for certifiably robust stump ensembles (Section 4).
- An extensive empirical evaluation, demonstrating the effectiveness of our approach and establishing a new state-of-the-art in a wide range of settings (Section 5).

2 Background on Randomized Smoothing

For a given base model $F: \mathbb{R}^d \rightarrow [C]$, classifying inputs to one of $C \in \mathbb{Z}^{\geq 2}$ classes, Randomized Smoothing (RS) is a method to construct a classifier $G: \mathbb{R}^d \rightarrow [C]$ with robustness guarantees. For a randomization scheme $\phi: \mathbb{R}^d \rightarrow \mathbb{R}^d$, we define the success probability $p_y := \mathbb{P}_{\mathbf{x}' \sim \phi(\mathbf{x})}[F(\mathbf{x}') = y]$ and $G(\mathbf{x}) := \arg \max_{c \in [C]} p_y$. Depending on the choice of ϕ , we obtain different certificates of the form:

Theorem 2.1 (Adapted from Cohen et al. [24], Yang et al. [25]). *If $\mathbb{P}(F(\phi(\mathbf{x})) = y) := p_y \geq \underline{p}_y$ and $\underline{p}_y > 0.5$, then $G(\mathbf{x} + \delta) = y$ for all δ satisfying $\|\delta\|_p < R$ with $R := \rho(\underline{p}_y)$.*

In particular, we present two instantiations that we utilize throughout this paper in Table 1, where Φ^{-1} is the inverse Gaussian CDF. Similar results, yielding other ℓ_p -norm certificates, can be derived for a wide range of input randomization schemes [25, 26]. Note that, by using more information than just \underline{p}_y , e.g., p_c for the runner-up class c , tighter certificates can be obtained [24, 27]. Once \underline{p}_y is computed, we can directly calculate the certifiable radius $R := \rho(\underline{p}_y)$. For a broader overview of variants of Randomized Smoothing, please refer to Section 6.

Table 1: Randomized Smoothing guarantees.

	$\phi(\mathbf{x})$	$R := \rho(\underline{p}_y)$
ℓ_1	$\mathbf{x} + \text{Unif}([- \lambda, \lambda]^d)$	$2\lambda(\underline{p}_y - \frac{1}{2})$
ℓ_2	$\mathbf{x} + \mathcal{N}(\mathbf{0}, \sigma \mathbf{I})$	$\sigma \Phi^{-1}(\underline{p}_y)$

For most choices of f and ϕ , the exact success probability p_y can not be computed efficiently. Thus a lower bound \underline{p}_y is estimated with confidence $1 - \alpha$ (typically $\alpha = 10^{-3}$) using Monte Carlo sampling and the Neyman-Pearson lemma [28]. Not only is this extremely computationally expensive, as typically 100 000 samples have to be evaluated per data point, but this also severely limits the maximum certifiable radius (see Fig. 6) and only yields probabilistic guarantees. Additionally, if the number of samples is not sufficient for the statistical test, the procedure will abstain from classifying.

In the following, we will show how considering a specific class of models f allows us to compute the success probability p_y exactly, overcoming these drawbacks, and thus invoke $\rho(p_y)$ to compute deterministic certificates over larger radii, orders of magnitude faster than RS.

3 Derandomized Smoothing for Decision Stump Ensembles

Tree-based models such as decision stump ensembles often combine exceptional performance on tabular data [1] with good interpretability, making them ideal for many real-world high-stakes applications. Here, we propose DRS, a method to equip them with deterministic robustness guarantees. In particular, we show that their structure permits an exact evaluation under isotropic input randomization schemes, such as those discussed in Section 2, and thus deterministic smoothing.

Stump Ensembles We define a decision stump as $f_m(\mathbf{x}) = \gamma_{l,m} + (\gamma_{r,m} - \gamma_{l,m})\mathbb{1}_{x_{j_m} > v_m}$, with leaf predictions $\gamma_{l,m}, \gamma_{r,m} \in [0, 1]$, split position v_m , and split variable j_m . We construct unweighted ensembles, particularly suitable for Smoothing [29], of M such stumps $\tilde{f}_M: \mathbb{R}^d \mapsto [0, 1]$ as

$$\tilde{f}_M(\mathbf{x}) := \frac{1}{M} \sum_{m=1}^M f_m(\mathbf{x}), \quad (1)$$

and treat them as a binary classifiers $\mathbb{1}_{\tilde{f}_M(\mathbf{x}) > 0.5}$. While our approach is extensible to multi-class classification by replacing the scalar leaf predictions γ with prediction-vectors, assigning a score per class, we focus on the binary case in this work.

Smoothed Stump Ensemble We now define a smoothed stump ensemble \bar{g}_M along the lines of Randomized Smoothing as discussed in Section 2, by evaluating \tilde{f}_M not only on the original input \mathbf{x} but rather on a whole distribution of $\mathbf{x}' \sim \phi(\mathbf{x})$:

$$\bar{g}_M(\mathbf{x}) := \mathbb{P}_{\mathbf{x}' \sim \phi(\mathbf{x})}[\tilde{f}_M(\mathbf{x}') > 0.5].$$

In this work, we consider randomization schemes $\phi(\mathbf{x})$ that are (i) isotropic, i.e., the dimensions of $\mathbf{x}' \sim \phi(\mathbf{x})$ are independently distributed, and (ii) permit an efficient computation of their marginal cumulative distribution functions (CDF). This includes a wide range of distributions, e.g., the Gaussian and Uniform distributions used in Table 1 and others commonly used for RS [25].

By denoting the model CDF as $\bar{\mathcal{F}}_{M,\mathbf{x}}(z) = \mathbb{P}_{\mathbf{x}' \sim \phi(\mathbf{x})}[\tilde{f}_M(\mathbf{x}') \leq z]$, we can alternatively define \bar{g}_M as $\bar{g}_M(\mathbf{x}) := 1 - \bar{\mathcal{F}}_{M,\mathbf{x}}(0.5)$, which will become useful later. For a label $y \in \{0, 1\}$ we obtain the success probability $p_y = |y - \bar{\mathcal{F}}_{M,\mathbf{x}}(0.5)|$ of predicting y for a sample from $\phi(\mathbf{x})$.

Meta-Stumps To evaluate p_y exactly as illustrated in Fig. 1, we group the stumps constituting an ensemble by their split variable j_m to obtain one *meta-stump* \tilde{f}_i per feature i . The key idea is that outputs of these meta-stumps are now independently distributed under isotropic input randomization (illustrated in Fig. 1 (b)), allowing us to aggregate them efficiently later on.

We showcase this in Fig. 2, where two stumps (f_1 and f_2) are combined into the meta-stump \tilde{f}_i . Formally, we have

$$\tilde{f}_i(\mathbf{x}) := \sum_{m \in \mathcal{I}_i} f_m(\mathbf{x}), \quad \mathcal{I}_i := \{m \in [M] \mid j_m = i\}, \quad (2)$$

define $M_i = |\mathcal{I}_i|$ and rewrite our ensemble as $\tilde{f}_M(\mathbf{x}) := \frac{1}{M} \sum_{i=1}^d \tilde{f}_i(x_i)$. Every meta-stump can be represented by its split positions $v_{i,j}$, sorted such that $v_{i,j} \leq v_{i,j+1}$, and its predictions $\gamma_{i,j} = \sum_{t=1}^{j-1} \gamma_{r,t} + \sum_{t=j}^{|\mathcal{I}_i|} \gamma_{l,m}$ on each of the resulting $|\mathcal{I}_i| + 1$ regions, written as $(\gamma, v)_i$.

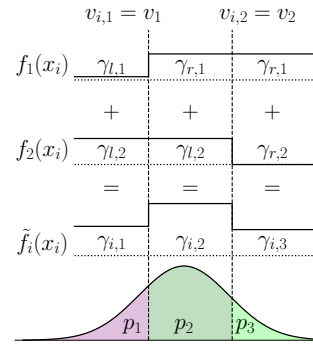


Figure 2: A meta-stump constructed from two stumps.

Algorithm 1 Stump Ensemble PDF computation via Dynamic Programming

```

function COMPUTEPDF( $\{(\Gamma, \mathbf{v})_i\}_{i=1}^d, \mathbf{x}, \phi$ )
  pdf[i][t] = 0 for  $t \in [M \cdot \Delta + 1], i \in [d]$ 
  pdf[0][0] = 1 ▷ For 0 stumps all probability mass is on 0
  for  $i = 1$  to  $d$  do
    for  $j = 1$  to  $M_i$  do
      for  $t = 0$  to  $M \cdot \Delta + 1 - \Gamma_{i,j}$  do
        pdf[i][t +  $\Gamma_{i,j}$ ] = pdf[i][t +  $\Gamma_{i,j}$ ] + pdf[i - 1][t] ·  $\mathbb{P}_{x'_i \sim \phi(\mathbf{x})}[v_{i,j-1} < x'_i \leq v_{i,j}]$ 
  return pdf
  
```

CDF Computation Now we leverage the independence of our meta-stumps’ output distributions under an isotropic input randomization scheme ϕ to compute the PDF of their ensemble efficiently via dynamic programming (DP) (illustrated in Fig. 1 (c) and explained below). Given its PDF, we can trivially compute the ensemble’s CDF $\bar{\mathcal{F}}_{M,\mathbf{x}}$, allowing us to evaluate the smoothed model exactly (illustrated in Fig. 1 (d)). This efficient CDF computation constitutes the core of DRS.

In more detail, we observe that the PDF of a stump ensemble is the convex sum of exponentially many ($\mathcal{O}((\max_i \mathcal{I}_i)^d)$) Dirac delta distributions. To avoid this exponential blow-up, we discretize all leaf predictions γ to a grid of Δ values (typically $\Delta = 100$), when constructing the smoothed model \bar{g}_M . For each $\gamma_{i,j}$, we define a corresponding $\Gamma_{i,j} \in \{0, \dots, M_i \cdot \Delta\}$ such that $\gamma_{i,j} = \frac{\Gamma_{i,j}}{\Delta}$. Now, we construct a DP-table, where every entry pdf[i][t] corresponds to the weight of the Dirac delta at position $\frac{t}{\Delta M}$ after considering the first i meta-stumps (in any fixed but arbitrary order). We outline the PDF computation in Algorithm 1. After initially allocating all probability mass to $t = 0$, we account for the effect of the i^{th} meta-stump, by updating the i^{th} row in the DP-table with $\text{pdf}[i][t] = \sum_j p_j \text{pdf}[i-1][t - \Gamma_{i,j}]$ where p_j is the probability $\mathbb{P}_{x'_i \sim \phi(\mathbf{x})}[v_{i,j-1} < x'_i \leq v_{i,j}]$ of the randomized x'_i lying between $v_{i,j-1}$ and $v_{i,j}$ (padded with $-\infty$ and ∞ on the left and right, respectively). This is illustrated in Fig. 2. After termination, the last line of the DP-table pdf[d] contains the full PDF (see Fig. 1(c)). Formally we summarize this in the theorem below, delaying a formal proof to App. A.1:

Theorem 3.1. For $z \in [0, 1]$, $\bar{\mathcal{F}}_{M,\mathbf{x}}(z) = \sum_{t=0}^{\lfloor zM\Delta \rfloor} \text{pdf}[d][t]$ describes the exact CDF and thus success probability $p_y = \mathbb{P}_{\mathbf{x}' \sim \phi(\mathbf{x})}[\bar{f}_M(\mathbf{x}') = y] = |y - \bar{\mathcal{F}}_{M,\mathbf{x}}(0.5)|$ for $y \in \{0, 1\}$.

Note that the presented algorithm is slightly simplified, and we actually only have to track the range of non-zero entries of one row of the DP-table. This allows us to compute the full PDF and thus certificates for smoothed stump ensembles very efficiently, e.g., taking only around 1.2 s total for the MNIST 2 vs. 6 task (around 2,000 data points and over 500 stumps).

Certification Recall from Section 2 that, given the success probability p_y , robustness certification for ℓ_p -norm bounded perturbations reduces to computing the maximal certifiable robustness radius $R = \rho(p_y)$. For all popular ℓ_p -norms, ρ (and its inverse ρ^{-1} ; used shortly) can be either evaluated symbolically [24, 25] or precomputed efficiently [30, 31], such that the core challenge of certification becomes computing (a lower bound to) p_y , which we solve efficiently via Theorem 3.1. Alternatively, for a given target radius r , we need to check whether $p_y \geq \rho^{-1}(r)$ by equivalently calculating

$$\bar{g}_{M,r}(\mathbf{x}) = \bar{\mathcal{F}}_{M,\mathbf{x}}^{-1}(z) \quad z = \begin{cases} 1 - \rho^{-1}(r) & \text{if } y = 1 \\ \rho^{-1}(r) & \text{if } y = 0 \end{cases}, \quad (3)$$

and checking $\bar{g}_{M,r}(\mathbf{x}) > 0.5$. This corresponds to asserting that class y is predicted at least z percent of the time. Here, the inverse CDF $\bar{\mathcal{F}}_{M,\mathbf{x}}^{-1}(z)$ can be efficiently evaluated using the step-wise $\bar{\mathcal{F}}_{M,\mathbf{x}}$ computed via Theorem 3.1. We will see in Section 4 that this view is useful when training stump ensembles for certifiability. Finally, we want to highlight that this approach can be used with all common randomization schemes yielding certificates for different ℓ_p -norm bounded adversaries.

Categorical Variables & Joint Certificates For practical applications, it is essential to handle both numerical and categorical features jointly. To consider a categorical feature $x_i \in \{1, \dots, d_i\}$ in our stump ensemble, we construct a d_i -ary stump $\tilde{f}_i: [d_i] \rightarrow [0, 1]$ returning a value $\gamma_{i,j}$ corresponding to each of the d_i categorical values and treated as a meta-stump with $M_i = 1$ for normalization.

To provide certificates in this setting, we propose a novel scheme combining an arbitrary ℓ_p -norm certificate of radius r_p over all numerical features, computed as discussed above, with an ℓ_0 certificate of radius r_0 over all categorical features \mathcal{C} , computed using an approach adapted from Wang et al. [23]. Conceptually, we compute the worst case effect of every individual categorical variable independently, greedily aggregate these worst case effects, and account for them in our ensemble’s CDF.

Given a meta-stump’s prediction on a concrete sample $q_i = \tilde{f}_i(x_i)$ as well as its maximal and minimal output u_i and l_i , respectively, we compute the maximum and minimum perturbation effect to $\bar{\delta}_i = \frac{u_i - q_i}{M}$ and $\underline{\delta}_i = \frac{l_i - q_i}{M}$, respectively. Given the set of categorical features \mathcal{C} , we can compute the worst-case effect when perturbing at most r_0 samples as

$$\bar{\delta}_{r_0} = \max_{\mathcal{R}} \sum_{i \in \mathcal{R}} \bar{\delta}_i, \quad \text{s.t. } |\mathcal{R}| \leq r_0, \mathcal{R} \subseteq \mathcal{C}$$

by greedily picking the r_0 largest $\bar{\delta}_i$. For $\underline{\delta}_{r_0}$ we proceed analogously. Shifting the CDF, computed as above, by $\bar{\delta}$ and $\underline{\delta}$ for samples with labels $y = 0$ and $y = 1$, respectively, before computing the success probability p_y , allows us to account for the worst-case categorical perturbations exactly. We illustrate this for a sample with $y = 0$ in Fig. 3, where we show the CDFs obtained by all possible perturbations of at most r_0 categorical variables, bounded to the right by those obtained by shifting the original by $\bar{\delta}_{r_0}$. Note that here no smoothing over the categorical variables is done or required, making inference trivial.

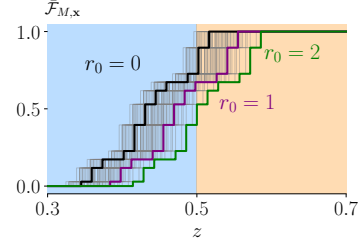


Figure 3: CDF shifted by the effect of categorical feature perturbations.

4 Training for and with Derandomized Smoothing

To obtain large certified radii via smoothing, the base model has to be robust to the chosen randomization scheme. To train robust decision stump ensembles, we propose a robust MLE optimality criterion for individual stumps (Section 4.1) and two boosting schemes for whole ensembles (Section 4.2).

4.1 Independently MLE-Optimal Stumps

To train an individual stump $f_m(\mathbf{x}) = \gamma_{l,m} + (\gamma_{r,m} - \gamma_{l,m})\mathbb{1}_{x_{j_m} > v_m}$, its split feature j_m , split position v_m , and leaf predictions $\gamma_{l,m}, \gamma_{r,m}$ have to be determined. We choose them in an MLE-optimal fashion with respect to the randomization scheme ϕ , starting with v_m , as follows: We consider the probabilities $p_{l,i} = \mathbb{P}_{\mathbf{x}' \sim \phi(\mathbf{x}_i)}[x'_{j_m} \leq v_m]$ and $p_{r,i} = 1 - p_{l,i}$ of \mathbf{x}'_i lying to the left or the right of v_m , respectively, under the input randomization scheme ϕ . For an i.i.d. dataset with n samples $(\mathbf{x}_i, y_i) \sim (\mathcal{X}, \mathcal{Y})$, we define the probabilities $p_j^y = \frac{1}{n} \sum_{\{i|y_i=y\}} p_{j,i}$ of picking the $j \in \{l, r\}$ leaf, conditioned on the target label, and $p_j = p_j^0 + p_j^1$ as their sum to compute the entropy impurity H_{entropy} [32] as

$$H_{\text{entropy}} = - \sum_{j \in \{l, r\}} p_j \sum_{y \in \{0, 1\}} \frac{p_j^y}{p_j} \log \left(\frac{p_j^y}{p_j} \right).$$

We then choose the v_m approximately minimizing H_{entropy} via line-search. After fixing v_m this way, we compute the MLE-optimal leaf predictions $\gamma_l^{\phi, \text{MLE}}$ and $\gamma_r^{\phi, \text{MLE}}$ as:

$$\begin{aligned} \gamma_l^{\phi, \text{MLE}}, \gamma_r^{\phi, \text{MLE}} &= \arg \max_{\gamma_l, \gamma_r} \mathbb{P}[\mathcal{Y} \mid \phi(\mathcal{X}), f_m] = \arg \max_{\gamma_l, \gamma_r} \sum_{i=1}^n \mathbb{E}_{\mathbf{x}' \sim \phi(\mathbf{x}_i)} [\log \mathbb{P}[y_i \mid \mathbf{x}', f_m]] \\ &= \arg \max_{\gamma_l, \gamma_r} \sum_{i \in \{i|y_i=0\}} p_{l,i} \log(1 - \gamma_l) + p_{r,i} \log(1 - \gamma_r) \\ &\quad + \sum_{i \in \{i|y_i=1\}} p_{l,i} \log(\gamma_l) + p_{r,i} \log(\gamma_r) \\ &= \arg \max_{\gamma_l, \gamma_r} p_l^0 \log(1 - \gamma_l) + p_r^0 \log(1 - \gamma_r) + p_l^1 \log(\gamma_l) + p_r^1 \log(\gamma_r), \end{aligned}$$

where the second line is obtained by splitting the sum over samples by class and explicitly computing the expectation. We solve the maximization problem by setting the first derivatives $\frac{\partial}{\partial \gamma_l}$ and $\frac{\partial}{\partial \gamma_r}$ of our optimization objective to zero and checking its Hessian to confirm that

$$\gamma_l^{\phi^{\text{MLE}}} = \frac{p_l^1}{p_l^1 + p_l^0} \quad \gamma_r^{\phi^{\text{MLE}}} = \frac{p_r^1}{p_r^1 + p_r^0} \quad (4)$$

are indeed maxima. We show in App. A.2 that $\gamma_l^{\phi^{\text{MLE}}}$, $\gamma_r^{\phi^{\text{MLE}}}$, and v_m are even jointly MLE-optimal, when v_m is chosen as the exact instead of an approximate minimizer of the entropy impurity.

Ensembling To train an ensemble of independently MLE-optimal decision stumps, we sequentially train one stump for every feature $j_m \in [d]$ and construct an ensemble with equal weights, rejecting stumps with an entropy impurity H_{entropy} above a predetermined threshold.

4.2 Boosting Stump Ensembles for Certifiable Robustness

Decision stumps trained this way maximize the expected likelihood under the chosen randomization scheme. Assuming (due to the law of large numbers) a Gaussian output distribution, this corresponds to optimizing for the median output, which determines the clean prediction. However, certified correctness at a given radius r is determined by the prediction $y'(\mathbf{x}, r) = \bar{\mathcal{F}}_{m-1, \mathbf{x}}^{-1}(z(r))$ at the $z(r) := |y - \rho^{-1}(r)|$ percentile of the output distribution. Where we call y' the *certifiable prediction*, as certification is now equivalent to checking $y = \mathbb{1}_{y'(\mathbf{x}, r) > 0.5}$ (Eq. (3)). This difference is illustrated in Fig. 4, where the clean prediction is correct (class 1) while the certifiable prediction is incorrect. To align our training objective better with certified accuracy, we propose two novel boosting schemes along the lines of the popular TREEBOOST [33] and ADABOOST [34].

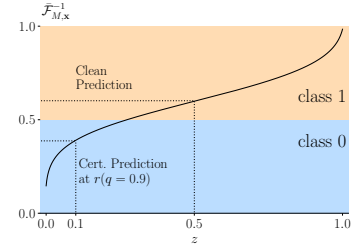


Figure 4: Inverse CDF $\bar{\mathcal{F}}_M^{-1}$

Gradient Boosting for Certifiable Robustness The key idea of gradient boosting is to compute the gradient of a loss function with respect to an ensemble’s outputs and then add a model to the ensemble, making a prediction along this gradient direction. Implementing this idea, we adapt TREEBOOST [33] to propose ROB TREEBOOST: At a high level, we add stumps to the ensemble, which aim to predict the residual between the target label and the current certifiable prediction. Concretely, to add the m^{th} stump to our ensemble, we begin by computing the current ensemble’s certifiable predictions $y'(r)$ at a target radius r and then defining the pseudo labels $\tilde{y} = y - y'(r)$ as the residual between the target labels y and the certifiable predictions $y'(r)$. This yields a regression problem, which we tackle by choosing a feature j_m and split threshold v_m (approximately) minimizing MSE impurity under input randomization before computing $\gamma_{l,m}$ and $\gamma_{r,m}$ as approximate minimizers of the cross-entropy loss over the whole ensemble. Please see App. A.3 for a more detailed discussion of ROB TREEBOOST.

Adaptive Boosting for Certifiable Robustness The key idea of adaptive boosting is to build an ensemble by iteratively training models, weighted based on their error rate, while adapting sample weights based on whether they are classified correctly. We build on ADABOOST [34] to propose ROB ADABOOST: We construct an ensemble of K stump ensembles via hard voting, where every ensemble is weighted based on its certifiable accuracy. To train a new ensemble, we increase the weights of all samples that are currently not classified certifiably correct at a given radius r . We choose stump ensembles instead of individual stumps as base classifiers because single stumps can not reach the success probabilities under input randomization required for certification. To compute the certifiable radius for such an ensemble \bar{F}_K , we compute the certifiable radii R^k of the individual stump ensembles \bar{F}_M^k , sort them in decreasing order such that $R^k \geq R^{k+1}$ and obtain the largest radius R^k such that the weights of the first k ensembles sum up to more than half of the total weights. Please see App. A.4 for a more detailed discussion of ROB ADABOOST.

5 Experimental Evaluation

In this section, we empirically demonstrate the effectiveness of DRS in a wide range of settings. We show that DRS significantly outperforms the current state-of-the-art for certifying tree-based models on established benchmarks, using only numerical features (Section 5.1), before highlighting its novel ability to obtain joint certificates on a set of new benchmarks (Section 5.2). Finally, we perform an ablation study, investigating the effect of DRS’s key components (Section 5.3).

Table 2: Natural accuracy (NAC) [%] and certified accuracy (CA) [%] with respect to ℓ_1 - and ℓ_2 -norm bounded perturbations. Results for Wang et al. [23] as reported by them. Larger is better.

Perturbation	Dataset	Radius r	Wang et al. [23]		Ours (Independent)		Ours (Boosting)	
			NAC	CA	NAC	CA	NAC	CA
ℓ_1 -norm	BREASTCANCER	1.0	98.5	64.2	100.0	81.0	100.0	83.9
	DIABETES	0.05	72.7	68.2	76.0	69.5	77.9	72.1
	FMNIST-SHOES	0.5	87.6	67.8	85.8	83.3	87.2	84.2
	MNIST 1 vs. 5	1.0	95.5	83.8	96.6	94.1	99.3	98.1
	MNIST 2 vs. 6	1.0	92.3	66.5	96.3	93.9	96.6	94.1
ℓ_2 -norm	BREASTCANCER	0.7	91.2	60.6	100.0	75.2	100.0	82.5
	DIABETES	0.05	-	-	77.3	68.2	79.9	71.4
	FMNIST-SHOES	0.4	75.5	51.5	86.8	81.2	91.0	84.5
	MNIST 1 vs. 5	0.8	95.6	63.4	95.8	91.6	99.2	96.3
	MNIST 2 vs. 6	0.8	86.3	23.0	96.3	89.6	96.3	89.6

Experimental Setup We implement our approach in PyTorch [35] and evaluate it on Intel Xeon Gold 6242 CPUs and an NVIDIA RTX 2080Ti. We compare to prior work on the DIABETES [36], BREASTCANCER [37], FMNIST-SHOES [38], MNIST 1 vs. 5 [39], and MNIST 2 vs. 6 [39] datasets and are the first to provide joint certificates of categorical and numerical features, demonstrated on the ADULT [37] and CREDIT [37] datasets. For a more detailed description of the experimental setup, please refer to App. B.

5.1 Certification for Numerical Features

In Table 2, we compare the certified accuracies obtained via DRS on ensembles of independently MLE optimal stumps (Independent) or boosted stump ensembles (Boosting) to the current state-of-the-art, Wang et al. [23], using established benchmarks [23].

Independently MLE Optimal Stumps We first consider stump ensembles trained without boosting as described in Section 4.1 and observe that DRS obtains higher certified accuracies in all settings and higher natural accuracies in most. For example, on MNIST 2 vs. 6, we increase the certified accuracy at an ℓ_2 radius of $r_2 = 0.8$ from 23.0% to 89.6%, almost quadrupling it compared to Wang et al. [23], while also improving natural accuracy from 86.3% to 96.3%.

Boosting for Certified Accuracy Leveraging the boosting techniques introduced in Section 4.2, ROBTREEBOOST for BREASTCANCER and DIABETES and ROBADA BOOST for FMNIST-SHOES, MNIST 1 vs. 5, and MNIST 2 vs. 6, we increase certifiable and natural accuracies even further in most settings. For example, compared to our independently trained stump ensemble, we improve the certified accuracy for MNIST 1 vs. 5 at an ℓ_1 -radius of $r_1 = 1.0$ from 94.1% to 98.1% and for BREASTCANCER at an ℓ_2 -radius of $r_2 = 0.7$ from 75.2% to 82.5%.

5.2 Joint Certificates for Categorical and Numerical Features

In Table 3, we compare models using only numerical, only categorical, or both types of features with regards to their balanced certified accuracy (BCA) (accounting for class frequency) at different combinations of ℓ_2 - and ℓ_0 -radii for numerical and categorical features, respectively. We observe that models using both categorical and numerical features perform notably better on clean data, highlighting the importance of utilizing and thus also certifying them in combination. Moreover, categorical features make the model significantly more robust to ℓ_2 perturbations, e.g., at ℓ_2 -radii > 0.75 , they improve certified accuracies, even when 2 categorical features (of only 8 and 7 for ADULT and CREDIT, respectively) are adversarially perturbed. We visualize this in Fig. 5, showing BCA over ℓ_2 -perturbation radius and confirm that the model utilizing only numerical features (dotted line) loses accuracy much quicker with perturbation magnitude than the model leveraging categorical variables (solid lines). As we are the first to tackle this setting, we do not compare to other methods but provide more detailed experiments in App. C.1.

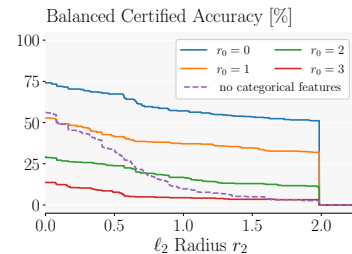


Figure 5: Effect of ℓ_0 -perturbations on ℓ_2 -robustness for CREDIT.

Table 3: Balanced certified accuracy (BCA) [%] under joint ℓ_0 - and ℓ_2 -perturbations of categorical and numerical features, respectively, depending on whether model uses categorical and/or numerical features. The balanced natural accuracy is the BCA at radius $r = 0.0$. Larger is better.

Dataset	Categorical Features	ℓ_0 Radius r_0	BCA without Numerical Features	BCA with Numerical Features at ℓ_2 Radius r_2						
				0.00	0.25	0.50	0.75	1.00	1.25	1.50
ADULT	no	-	-	74.9	65.7	42.4	27.4	14.5	8.9	5.1
		0	76.6	77.5	73.9	68.1	63.3	48.7	40.7	35.2
	yes	1	57.4	66.0	61.7	53.9	47.4	34.3	26.6	21.8
		2	33.5	51.4	46.2	37.5	29.3	21.5	17.1	13.4
		3	8.9	36.7	31.4	24.1	15.4	10.3	8.1	5.7
CREDIT	no	-	-	56.1	44.5	33.3	17.7	9.7	7.2	5.0
		0	70.7	74.1	70.3	67.3	59.7	57.1	54.9	53.4
	yes	1	48.2	52.7	47.7	41.7	38.3	37.1	35.1	34.7
		2	26.4	29.3	26.0	23.8	19.2	16.8	13.5	13.0
		3	7.8	13.6	10.3	7.8	4.9	4.4	3.9	3.4

5.3 Ablation Study

We first illustrate the effectiveness of our derandomization approach, before demonstrating the benefit of training with our MLE optimality criterion and investigating the effect of the noise level on DRS.

Derandomized vs Randomized Smoothing In Fig. 6, we compare DRS, (dotted line) and sampling-based RS (solid lines), with respect to certified accuracy over ℓ_2 radii. We observe that the sampling-based estimation of the success probability in RS significantly limits the obtained certifiable radii. While this effect is particularly pronounced for small sample counts n , increasing the maximum certifiable radius, visible as the sudden drop in certifiable accuracy, requires an exponentially increasing number of samples, making the certification of large radii intractable. DRS, in contrast, can compute exact success probabilities and thus deterministic guarantees for much larger radii, yielding a 33.1% increase in ACR compared to using $n = 100\,000$ samples. Additionally, DRS is multiple orders of magnitude faster than RS, here, only requiring approximately $6.45 \cdot 10^{-4}$ s per sample. For more extensive experiments, please refer to App. C.2.

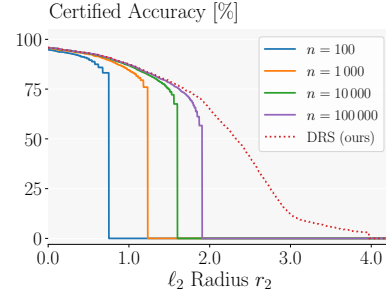


Figure 6: DRS vs. RS with various sample counts n on MNIST 1 vs. 5.

MLE Optimality Criterion In Table 4, we evaluate our robust MLE optimality criterion (MLE) by comparing it to the standard entropy criterion applied to samples drawn from the input randomization scheme (Sampling) or the clean data (Default). We observe that the ensemble trained on the clean data (Default) suffers from a mode collapse when evaluated under noise. In contrast, both approaches considering the input randomization perform much better, with our robust MLE approach outperforming sampling by a significant margin, especially at large radii. For more extensive experiments, please refer to App. C.3.

Table 4: Comparison of training with the exact distribution (MLE), randomly perturbed data (Sampling), or clean data (Default) on BREASTCANCER for $\sigma = 1$.

Method	ACR	Certified Accuracy [%] at Radius r			
		0.0	0.25	0.5	0.75
MLE (Ours)	0.675	100.0	97.1	86.1	30.7
Sampling	0.567	99.3	95.6	75.2	8.8
Default	0.356	26.3	25.5	25.5	25.5

Effect of Noise Level In Fig. 7, we compare the certified accuracy over ℓ_1 -radii for a range of different noise magnitudes λ and ensembles of independently MLE optimal stumps. We observe that at large perturbation magnitudes, we obtain stumps that ‘think outside the (hyper-)box’, i.e., choose splits outside of the original data range, making their ensembles exceptionally robust, even at large radii. In particular, we obtain a certifiable accuracy of 87.3% at radius $r_1 = 4.0$, while the state-of-the-art achieves only 83.8% at $r_1 = 1.0$ [23]. We provide more experiments for varying noise magnitudes in App. C.4.

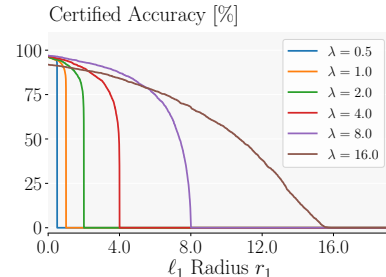


Figure 7: Comparing DRS for various noise levels λ on MNIST 1 vs. 5.

6 Related Work

(De-)Randomized Smoothing Probabilistic certification methods [40, 41, 24] are a popular approach for obtaining robustness certificates for a wide range of tasks [31, 42–45] and threat models [25, 26, 46, 47, 27, 30, 31, 42, 48–52]. These methods follow the general blueprint discussed in Section 2 and consider arbitrary base classifiers, though specially trained [53–55], and can thus, in contrast to our work, not leverage their structure. Specifically designed randomization schemes [50, 52] enable efficient enumeration and thus a deterministic certificate for, e.g., patch attacks or ℓ_1 -norm perturbations. In contrast to these approaches, we permit arbitrary isotropic continuous randomization schemes, allowing us to leverage comprehensive results on RS to obtain robustness guarantees against a wide range of ℓ_p -norm bounded adversaries [25].

Certification and Training of Tree-Based Models In the setting of ℓ_∞ robustness, where every feature can be perturbed independently, various methods have been proposed to train [4, 22, 56, 57] and certify [22, 58–60] robust decision trees and stumps. However, ℓ_∞ robust models are still vulnerable to other ℓ_p norm perturbations [61, 62], which cover many realistic perturbations better and are the focus of this work. There, the admissible perturbation of one feature depends on the perturbations of all others, making the above approaches leveraging their independence not applicable.

On the other hand, Kantchelian et al. [63] discuss complete robustness certification of tree ensembles in the ℓ_p -norm setting via MILP. However, this approach is intractable in most settings due to its Co-NP-complete complexity. Wang et al. [23] propose an efficient but incomplete DP-based certification algorithm for stump ensembles based on over-approximating the maximum perturbation effect in the ℓ_p -norm setting. While similarly fast as our approach, we show empirically in Section 5 that DRS obtains significantly stronger certificates. Wang et al. [23] further introduce an incomplete certification algorithm for tree ensembles, which is based on computing the distance between the pre-image of all trees’ leaves and the original sample. As they report significantly worse results using this approach than with stump ensembles, we omit a detailed comparison.

7 Limitations and Societal Impact

Limitations While able to handle arbitrary stump ensembles, and being extensible to arbitrary decision trees, DRS can not handle arbitrary ensembles of decision trees. However, as these have been shown to be significantly more sensitive to ℓ_p -norm perturbations than stump ensembles [23], we believe this limitation to be of little practical relevance. Further, like all Smoothing-based approaches, we construct a smoothed model from a base classifier and only obtain robustness guarantees for the former. In contrast to standard Randomized Smoothing approaches, we can, however, evaluate the smoothed model exactly and efficiently.

Societal Impact As our contributions improve certified accuracy and certification radii while retaining high natural accuracy, they could help make real-world AI systems more robust and thus generally amplify both any positive or negative societal effects. Further, while we achieve state-of-the-art results, these may not be sufficient to guarantee robustness in real-world deployment and could give practitioners a false sense of security, leading to them relying more on our models than is justified.

8 Conclusion

We propose DRS, a (De-)Randomized Smoothing approach to robustness certification, enabling joint deterministic certificates over numerical and categorical variables for decision stump ensembles by leveraging their structure to compute their exact output distributions for a given input randomization scheme. The key insight enabling this is that this output distribution can be efficiently computed by aggregating independent distributions associated with the individual features used by the ensemble. We additionally propose a robust MLE optimality criterion for training individual decision stumps and two boosting schemes improving an ensemble’s certifiable accuracy. Empirically, we demonstrate that DRS significantly outperforms the state-of-the-art for tree-based models in a wide range of settings, obtaining up to 4-fold improvements in certifiable accuracy.

References

- [1] R. Shwartz-Ziv and A. Armon, “Tabular data: Deep learning is not all you need,” *Information Fusion*, vol. 81, 2022.
- [2] B. Biggio, I. Corona, D. Maiorca, B. Nelson, N. Srndic, P. Laskov, G. Giacinto, and F. Roli, “Evasion attacks against machine learning at test time,” in *Machine Learning and Knowledge Discovery in Databases - European Conference, ECML PKDD 2013, Prague, Czech Republic, September 23-27, 2013, Proceedings, Part III*, vol. 8190, 2013.
- [3] C. Szegedy, W. Zaremba, I. Sutskever, J. Bruna, D. Erhan, I. J. Goodfellow, and R. Fergus, “Intriguing properties of neural networks,” in *Proc. of ICLR*, 2014.
- [4] H. Chen, H. Zhang, D. S. Boning, and C. Hsieh, “Robust decision trees against adversarial examples,” in *Proc. of ICML*, vol. 97, 2019.
- [5] F. Cartella, O. Anunciação, Y. Funabiki, D. Yamaguchi, T. Akishita, and O. Elshocht, “Adversarial attacks for tabular data: Application to fraud detection and imbalanced data,” in *Proceedings of the Workshop on Artificial Intelligence Safety 2021 (SafeAI 2021) co-located with the Thirty-Fifth AAAI Conference on Artificial Intelligence (AAAI 2021), Virtual, February 8, 2021*, vol. 2808, 2021.
- [6] Y. Mathov, E. Levy, Z. Katzir, A. Shabtai, and Y. Elovici, “Not all datasets are born equal: On heterogeneous tabular data and adversarial examples,” *Knowl. Based Syst.*, vol. 242, 2022.
- [7] G. Singh, T. Gehr, M. Püschel, and M. T. Vechev, “An abstract domain for certifying neural networks,” *Proc. ACM Program. Lang.*, vol. 3, no. POPL, 2019.
- [8] K. Xu, Z. Shi, H. Zhang, Y. Wang, K. Chang, M. Huang, B. Kailkhura, X. Lin, and C. Hsieh, “Automatic perturbation analysis for scalable certified robustness and beyond,” in *Advances in Neural Information Processing Systems 33: Annual Conference on Neural Information Processing Systems 2020, NeurIPS 2020, December 6-12, 2020, virtual*, 2020.
- [9] T. Gehr, M. Mirman, D. Drachler-Cohen, P. Tsankov, S. Chaudhuri, and M. T. Vechev, “AI2: safety and robustness certification of neural networks with abstract interpretation,” in *2018 IEEE Symposium on Security and Privacy, SP 2018, Proceedings, 21-23 May 2018, San Francisco, California, USA*, 2018.
- [10] S. Wang, K. Pei, J. Whitehouse, J. Yang, and S. Jana, “Efficient formal safety analysis of neural networks,” in *Advances in Neural Information Processing Systems 31: Annual Conference on Neural Information Processing Systems 2018, NeurIPS 2018, December 3-8, 2018, Montréal, Canada*, 2018.
- [11] T. Weng, H. Zhang, H. Chen, Z. Song, C. Hsieh, L. Daniel, D. S. Boning, and I. S. Dhillon, “Towards fast computation of certified robustness for relu networks,” in *Proc. of ICML*, vol. 80, 2018.
- [12] E. Wong and J. Z. Kolter, “Provable defenses against adversarial examples via the convex outer adversarial polytope,” in *Proc. of ICML*, vol. 80, 2018.
- [13] G. Singh, T. Gehr, M. Mirman, M. Püschel, and M. T. Vechev, “Fast and effective robustness certification,” in *Advances in Neural Information Processing Systems 31: Annual Conference on Neural Information Processing Systems 2018, NeurIPS 2018, December 3-8, 2018, Montréal, Canada*, 2018.
- [14] M. N. Müller, G. Makarchuk, G. Singh, M. Püschel, and M. T. Vechev, “PRIMA: general and precise neural network certification via scalable convex hull approximations,” *Proc. ACM Program. Lang.*, vol. 6, no. POPL, 2022.
- [15] V. Tjeng, K. Y. Xiao, and R. Tedrake, “Evaluating robustness of neural networks with mixed integer programming,” in *Proc. of ICLR*, 2019.

- [16] S. Dathathri, K. Dvijotham, A. Kurakin, A. Raghunathan, J. Uesato, R. Bunel, S. Shankar, J. Steinhardt, I. J. Goodfellow, P. Liang, and P. Kohli, “Enabling certification of verification-agnostic networks via memory-efficient semidefinite programming,” in *Advances in Neural Information Processing Systems 33: Annual Conference on Neural Information Processing Systems 2020, NeurIPS 2020, December 6-12, 2020, virtual*, 2020.
- [17] R. Ehlers, “Formal verification of piece-wise linear feed-forward neural networks,” in *Automated Technology for Verification and Analysis - 15th International Symposium, ATVA 2017, Pune, India, October 3-6, 2017, Proceedings*, vol. 10482, 2017.
- [18] M. Mirman, T. Gehr, and M. T. Vechev, “Differentiable abstract interpretation for provably robust neural networks,” in *Proc. of ICML*, vol. 80, 2018.
- [19] M. Balunovic and M. T. Vechev, “Adversarial training and provable defenses: Bridging the gap,” in *Proc. of ICLR*, 2020.
- [20] A. Raghunathan, J. Steinhardt, and P. Liang, “Certified defenses against adversarial examples,” in *Proc. of ICLR*, 2018.
- [21] S. Gowal, K. Dvijotham, R. Stanforth, R. Bunel, C. Qin, J. Uesato, R. Arandjelovic, T. A. Mann, and P. Kohli, “On the effectiveness of interval bound propagation for training verifiably robust models,” *ArXiv preprint*, vol. abs/1810.12715, 2018.
- [22] M. Andriushchenko and M. Hein, “Provably robust boosted decision stumps and trees against adversarial attacks,” in *Advances in Neural Information Processing Systems 32: Annual Conference on Neural Information Processing Systems 2019, NeurIPS 2019, December 8-14, 2019, Vancouver, BC, Canada*, 2019.
- [23] Y. Wang, H. Zhang, H. Chen, D. S. Boning, and C. Hsieh, “On lp-norm robustness of ensemble decision stumps and trees,” in *Proc. of ICML*, vol. 119, 2020.
- [24] J. M. Cohen, E. Rosenfeld, and J. Z. Kolter, “Certified adversarial robustness via randomized smoothing,” in *Proc. of ICML*, vol. 97, 2019.
- [25] G. Yang, T. Duan, J. E. Hu, H. Salman, I. P. Razenshteyn, and J. Li, “Randomized smoothing of all shapes and sizes,” in *Proc. of ICML*, vol. 119, 2020.
- [26] D. Zhang, M. Ye, C. Gong, Z. Zhu, and Q. Liu, “Black-box certification with randomized smoothing: A functional optimization based framework,” in *Advances in Neural Information Processing Systems 33: Annual Conference on Neural Information Processing Systems 2020, NeurIPS 2020, December 6-12, 2020, virtual*, 2020.
- [27] K. D. Dvijotham, J. Hayes, B. Balle, Z. Kolter, C. Qin, A. György, K. Xiao, S. Gowal, and P. Kohli, “A framework for robustness certification of smoothed classifiers using f-divergences,” in *Proc. of ICLR*, 2020.
- [28] J. Neyman and E. S. Pearson, “Ix. on the problem of the most efficient tests of statistical hypotheses,” *Philosophical Transactions of the Royal Society of London. Series A, Containing Papers of a Mathematical or Physical Character*, vol. 231, no. 694-706, 1933.
- [29] M. Z. Horváth, M. N. Müller, M. Fischer, and M. T. Vechev, “Boosting randomized smoothing with variance reduced classifiers,” in *Proc. of ICLR*, 2022.
- [30] G. Lee, Y. Yuan, S. Chang, and T. S. Jaakkola, “Tight certificates of adversarial robustness for randomly smoothed classifiers,” in *Advances in Neural Information Processing Systems 32: Annual Conference on Neural Information Processing Systems 2019, NeurIPS 2019, December 8-14, 2019, Vancouver, BC, Canada*, 2019.
- [31] A. Bojchevski, J. Klicpera, and S. Günnemann, “Efficient robustness certificates for discrete data: Sparsity-aware randomized smoothing for graphs, images and more,” in *Proc. of ICML*, vol. 119, 2020.
- [32] B. Bustos, D. A. Keim, D. Saupe, T. Schreck, and D. V. Vranic, “Using entropy impurity for improved 3d object similarity search,” in *Proceedings of the 2004 IEEE International Conference on Multimedia and Expo, ICME 2004, 27-30 June 2004, Taipei, Taiwan*, 2004.

- [33] J. H. Friedman, “Greedy function approximation: a gradient boosting machine,” *Annals of statistics*, 2001.
- [34] Y. Freund and R. E. Schapire, “A decision-theoretic generalization of on-line learning and an application to boosting,” *J. Comput. Syst. Sci.*, vol. 55, no. 1, 1997.
- [35] A. Paszke, S. Gross, F. Massa, A. Lerer, J. Bradbury, G. Chanan, T. Killeen, Z. Lin, N. Gimelshein, L. Antiga, A. Desmaison, A. Köpf, E. Yang, Z. DeVito, M. Raison, A. Tejani, S. Chilamkurthy, B. Steiner, L. Fang, J. Bai, and S. Chintala, “Pytorch: An imperative style, high-performance deep learning library,” in *Advances in Neural Information Processing Systems 32: Annual Conference on Neural Information Processing Systems 2019, NeurIPS 2019, December 8-14, 2019, Vancouver, BC, Canada*, 2019.
- [36] J. W. Smith, J. E. Everhart, W. C. Dickson, W. C. Knowler, and R. S. Johannes, “Using the adap learning algorithm to forecast the onset of diabetes mellitus,” in *Annual Symposium on Computer Application in Medical Care*, 1988.
- [37] D. Dua and C. Graff, “UCI machine learning repository,” 2017.
- [38] H. X. an, “Fashion-mnist: a novel image dataset for benchmarking machine learnin,” *ArXiv preprint*, vol. abs/1708.07747, 2017.
- [39] Y. LeCun and C. Cortes, “MNIST handwritten digit database,” 1998.
- [40] B. Li, C. Chen, W. Wang, and L. Carin, “Certified adversarial robustness with additive noise,” in *Advances in Neural Information Processing Systems 32: Annual Conference on Neural Information Processing Systems 2019, NeurIPS 2019, December 8-14, 2019, Vancouver, BC, Canada*, 2019.
- [41] M. Lécuyer, V. Atlidakis, R. Geambasu, D. Hsu, and S. Jana, “Certified robustness to adversarial examples with differential privacy,” in *2019 IEEE Symposium on Security and Privacy, SP 2019, San Francisco, CA, USA, May 19-23, 2019*, 2019.
- [42] Z. Gao, R. Hu, and Y. Gong, “Certified robustness of graph classification against topology attack with randomized smoothing,” in *IEEE Global Communications Conference, GLOBECOM 2020, Virtual Event, Taiwan, December 7-11, 2020*, 2020.
- [43] P. Chiang, M. J. Curry, A. Abdelkader, A. Kumar, J. Dickerson, and T. Goldstein, “Detection as regression: Certified object detection with median smoothing,” in *Advances in Neural Information Processing Systems 33: Annual Conference on Neural Information Processing Systems 2020, NeurIPS 2020, December 6-12, 2020, virtual*, 2020.
- [44] M. Fischer, M. Baader, and M. T. Vechev, “Scalable certified segmentation via randomized smoothing,” in *Proc. of ICML*, vol. 139, 2021.
- [45] J. Jia, X. Cao, B. Wang, and N. Z. Gong, “Certified robustness for top-k predictions against adversarial perturbations via randomized smoothing,” in *Proc. of ICLR*, 2020.
- [46] M. Fischer, M. Baader, and M. T. Vechev, “Certified defense to image transformations via randomized smoothing,” in *Advances in Neural Information Processing Systems 33: Annual Conference on Neural Information Processing Systems 2020, NeurIPS 2020, December 6-12, 2020, virtual*, 2020.
- [47] L. Li, M. Weber, X. Xu, L. Rimanic, B. Kailkhura, T. Xie, C. Zhang, and B. Li, “Tss: Transformation-specific smoothing for robustness certification,” in *ACM CCS*, 2021.
- [48] B. Wang, J. Jia, X. Cao, and N. Z. Gong, “Certified robustness of graph neural networks against adversarial structural perturbation,” in *KDD '21: The 27th ACM SIGKDD Conference on Knowledge Discovery and Data Mining, Virtual Event, Singapore, August 14-18, 2021*, 2021.
- [49] J. Schuchardt, A. Bojchevski, J. Klicpera, and S. Günnemann, “Collective robustness certificates,” in *International Conference on Learning Representations*, 2021.

- [50] A. Levine and S. Feizi, “Robustness certificates for sparse adversarial attacks by randomized ablation,” in *The Thirty-Fourth AAAI Conference on Artificial Intelligence, AAAI 2020, The Thirty-Second Innovative Applications of Artificial Intelligence Conference, IAAI 2020, The Tenth AAAI Symposium on Educational Advances in Artificial Intelligence, EAAI 2020, New York, NY, USA, February 7-12, 2020*, 2020.
- [51] —, “(de)randomized smoothing for certifiable defense against patch attacks,” in *Advances in Neural Information Processing Systems 33: Annual Conference on Neural Information Processing Systems 2020, NeurIPS 2020, December 6-12, 2020, virtual*, 2020.
- [52] —, “Improved, deterministic smoothing for l_1 certified robustness,” in *Proc. of ICML*, vol. 139, 2021.
- [53] J. Jeong and J. Shin, “Consistency regularization for certified robustness of smoothed classifiers,” in *Advances in Neural Information Processing Systems 33: Annual Conference on Neural Information Processing Systems 2020, NeurIPS 2020, December 6-12, 2020, virtual*, 2020.
- [54] R. Zhai, C. Dan, D. He, H. Zhang, B. Gong, P. Ravikumar, C. Hsieh, and L. Wang, “MACER: attack-free and scalable robust training via maximizing certified radius,” in *Proc. of ICLR*, 2020.
- [55] H. Salman, J. Li, I. P. Razenshteyn, P. Zhang, H. Zhang, S. Bubeck, and G. Yang, “Provably robust deep learning via adversarially trained smoothed classifiers,” in *Advances in Neural Information Processing Systems 32: Annual Conference on Neural Information Processing Systems 2019, NeurIPS 2019, December 8-14, 2019, Vancouver, BC, Canada*, 2019.
- [56] S. Calzavara, C. Lucchese, G. Tolomei, S. A. Abebe, and S. Orlando, “Treant: training evasion-aware decision trees,” *Data Min. Knowl. Discov.*, vol. 34, no. 5, 2020.
- [57] D. Vos and S. Verwer, “Efficient training of robust decision trees against adversarial examples,” in *Proc. of ICML*, vol. 139, 2021.
- [58] H. Chen, H. Zhang, S. Si, Y. Li, D. S. Boning, and C. Hsieh, “Robustness verification of tree-based models,” in *Advances in Neural Information Processing Systems 32: Annual Conference on Neural Information Processing Systems 2019, NeurIPS 2019, December 8-14, 2019, Vancouver, BC, Canada*, 2019.
- [59] F. Ranzato and M. Zanella, “Abstract interpretation of decision tree ensemble classifiers,” in *The Thirty-Fourth AAAI Conference on Artificial Intelligence, AAAI 2020, The Thirty-Second Innovative Applications of Artificial Intelligence Conference, IAAI 2020, The Tenth AAAI Symposium on Educational Advances in Artificial Intelligence, EAAI 2020, New York, NY, USA, February 7-12, 2020*, 2020.
- [60] J. Törnblom and S. Nadjm-Tehrani, “An abstraction-refinement approach to formal verification of tree ensembles,” in *Computer Safety, Reliability, and Security - SAFECOMP 2019 Workshops, ASSURE, DECSoS, SASSUR, STRIVE, and WAISE, Turku, Finland, September 10, 2019, Proceedings*, vol. 11699, 2019.
- [61] L. Schott, J. Rauber, M. Bethge, and W. Brendel, “Towards the first adversarially robust neural network model on MNIST,” in *Proc. of ICLR*, 2019.
- [62] F. Tramèr and D. Boneh, “Adversarial training and robustness for multiple perturbations,” in *Advances in Neural Information Processing Systems 32: Annual Conference on Neural Information Processing Systems 2019, NeurIPS 2019, December 8-14, 2019, Vancouver, BC, Canada*, 2019.
- [63] A. Kantchelian, J. D. Tygar, and A. D. Joseph, “Evasion and hardening of tree ensemble classifiers,” in *Proc. of ICML*, vol. 48, 2016.

A Additional Theory

In this section, we provide additional theoretical results, omitted in the main paper due to space constraints. Concretely, in App. A.1 we provide a proof for Theorem 3.1 on the correctness of our PDF computation. In App. A.2, we show that γ_l , γ_r and v_m , computed as outlined in Section 4, are indeed jointly MLE-optimal. Finally, we provide more details on ROBTREEBOOST and ROBADA BOOST in App. A.3 and App. A.4, respectively.

A.1 PDF Computation

Here, we provide a proof for Theorem 3.1 on the correctness of our efficient PDF-computation, restated below for convenience.

Theorem 3.1. *For $z \in [0, 1]$, $\bar{\mathcal{F}}_{M,\mathbf{x}}(z) = \sum_{t=0}^{\lfloor zM\Delta \rfloor} \text{pdf}[d][t]$ describes the exact CDF and thus success probability $p_y = \mathbb{P}_{\mathbf{x}' \sim \phi(\mathbf{x})}[\bar{f}_M(\mathbf{x}') = y] = |y - \bar{\mathcal{F}}_{M,\mathbf{x}}(0.5)|$ for $y \in \{0, 1\}$.*

Proof. Let the random variable $\Gamma^{(i)}$ be the prediction of the i -th meta-stump, then we have by definition of the meta-stump $\mathbb{P}[\Gamma^{(i)} = \Gamma_{i,j}] = \mathbb{P}_{\mathbf{x}' \sim \phi(\mathbf{x})}[v_{i,j-1} < x'_i \leq v_{i,j}]$ (see Section 3). Note that, for presentational simplicity, we assume $\Gamma_{i,j} \neq \Gamma_{i,k}, \forall k \neq j$. Now, we first show by induction that $\text{pdf}[i]$ computes the exact PDF of $\sum_{l=1}^i \Gamma^{(l)}$ (Lemma 1), before showing how the CDF of the meta-stump ensemble follows.

Lemma 1. *Algorithm 1 computes $\text{pdf}[i][t] = \mathbb{P}\left[\sum_{l=1}^i \Gamma^{(l)} = t\right]$.*

Proof. We proceed by induction over i . In the base case, for $i = 0$, we directly have $\text{pdf}[0][0] = 1.0$ and $\text{pdf}[0][t] = 0.0$ for $t > 0$ by construction. Now the induction assumption is that $\text{pdf}[i-1][t] = \mathbb{P}\left[\sum_{l=1}^{i-1} \Gamma^{(l)} = t\right]$ for an arbitrary $i \leq d$ and all corresponding t . To compute the $\text{pdf}[i][t]$, we now have:

$$\begin{aligned} \text{pdf}[i][t] &= \sum_{j=1}^{M_i} \text{pdf}[i-1][t - \Gamma_{i,j}] \cdot \mathbb{P}_{\mathbf{x}' \sim \phi(\mathbf{x})}[v_{i,j-1} < x'_i \leq v_{i,j}] \\ &= \sum_{j=1}^{M_i} \mathbb{P}\left[\left(\sum_{l=1}^{i-1} \Gamma^{(l)}\right) = t - \Gamma_{i,j}\right] \cdot \mathbb{P}_{\mathbf{x}' \sim \phi(\mathbf{x})}[v_{i,j-1} < x'_i \leq v_{i,j}] \\ &= \sum_{j=1}^{M_i} \mathbb{P}\left[\left(\sum_{l=1}^i \Gamma^{(l)}\right) = t \mid \Gamma^{(i)} = \Gamma_{i,j}\right] \cdot \mathbb{P}\left[\Gamma^{(i)} = \Gamma_{i,j}\right] \\ &= \mathbb{P}\left[\left(\sum_{l=1}^i \Gamma^{(l)}\right) = t\right] \end{aligned}$$

where we first use the definition $\text{pdf}[i][t]$ according to Algorithm 1, followed by induction assumption, the independency of different meta-stumps and the law of total probability over j . \square

Now, we show how Theorem 3.1 directly follows from Lemma 1. Recall that $\gamma_{i,j} = \frac{\Gamma_{i,j}}{\Delta}$, where Δ is the number of discretization steps. Similarly to $\Gamma^{(i)}$, let $\gamma^{(i)}$ be the random variable describing the prediction of the i -th meta-stump. Using Lemma 1, we obtain

$$\begin{aligned} \bar{\mathcal{F}}_{M,\mathbf{x}}(z) &= \sum_{t=0}^{\lfloor zM\Delta \rfloor} \text{pdf}[d][t] \\ &= \sum_{t=0}^{\lfloor zM\Delta \rfloor} \mathbb{P}\left[\sum_{i=1}^d \Gamma^{(i)} = t\right] \end{aligned}$$

$$\begin{aligned}
&= \mathbb{P} \left[\sum_{i=1}^d \Gamma^{(i)} \leq \lfloor zM\Delta \rfloor \right] \\
&= \mathbb{P} \left[\sum_{i=1}^d \frac{\gamma^{(i)}}{M} M\Delta \leq \lfloor zM\Delta \rfloor \right] \\
&= \mathbb{P} \left[\sum_{i=1}^d \frac{\gamma^{(i)}}{M} \leq z \right] \\
&= \mathbb{P} [\bar{f}_M(\mathbf{x}) \leq z] .
\end{aligned}$$

Where the second to last step follows from the discretization of the leaf predictions leading to a piece-wise constant CDF. \square

A.2 MLE-Optimal Stumps

In this section, we extend the theory from Section 4.1, showing that the v_m , γ_l and γ_r computed as outlined there, are, in fact, jointly MLE-optimal.

Recall that an individual stump operating on feature j_m is characterized by three parameters: v_m , γ_l and γ_r . In Section 4.1, we show how to choose MLE-optimal γ_l and γ_r given v_m . It remains to show that if v_m minimizes the entropy impurity H_{entropy} , then $\gamma_l^{\phi, \text{MLE}}$, $\gamma_r^{\phi, \text{MLE}}$, and v_m are jointly MLE-optimal.

For an arbitrary split position v_m , we have the probabilities $p_{l,i}(v_m) = \mathbb{P}_{\mathbf{x}' \sim \phi(\mathbf{x}_i)}[x'_{j_m} \leq v_m]$ and $p_{r,i}(v_m) = 1 - p_{l,i}(v_m)$ of \mathbf{x}'_i lying to the left or the right of v_m , respectively, under the input randomization scheme ϕ . For an i.i.d. dataset with n samples $(\mathbf{x}_i, y_i) \sim (\mathcal{X}, \mathcal{Y})$, we define the probabilities $p_j^y(v_m) = \frac{1}{n} \sum_{\{i|y_i=y\}} p_{j,i}(v_m)$ of picking the $j \in \{l, r\}$ leaf, conditioned on the target label, and $p_j(v_m) = p_j^0(v_m) + p_j^1(v_m)$ as their sum. Now, we compute the entropy impurity H_{entropy} [32] as

$$\begin{aligned}
H_{\text{entropy}}(v_m) &= - \sum_{j \in \{l, r\}} p_j(v_m) \sum_{y \in \{0, 1\}} \frac{p_j^y(v_m)}{p_j(v_m)} \log \left(\frac{p_j^y(v_m)}{p_j(v_m)} \right) \\
&= - \sum_{j \in \{l, r\}} \sum_{y \in \{0, 1\}} p_j^y(v_m) \log \left(\frac{p_j^y(v_m)}{p_j(v_m)} \right) .
\end{aligned}$$

Similarly, let $\gamma_l^{\phi, \text{MLE}}(v_m)$ and $\gamma_r^{\phi, \text{MLE}}(v_m)$ be the MLE-optimal predictions given v_m , as computed in Section 4.1. We formalize our statement as follows in Theorem A.1:

Theorem A.1. *Given an i.i.d. dataset with n samples $(\mathbf{x}_i, y_i) \sim (\mathcal{X}, \mathcal{Y})$, let $v_m^* := \arg \min_{v_m} H_{\text{entropy}}(v_m)$, $\gamma_l(v_m^*) = \frac{p_l^1(v_m^*)}{p_l^1(v_m^*) + p_l^0(v_m^*)}$ and $\gamma_r(v_m^*) = \frac{p_r^1(v_m^*)}{p_r^1(v_m^*) + p_r^0(v_m^*)}$. Then v_m^* , γ_l and γ_r are jointly MLE-optimal with respect to that dataset.*

Proof. Similarly to Section 4.1, but also optimizing over v_m , we obtain:

$$\begin{aligned}
v_m^{\phi, \text{MLE}}, \gamma_l^{\phi, \text{MLE}}, \gamma_r^{\phi, \text{MLE}} &= \arg \max_{v_m, \gamma_l, \gamma_r} \mathbb{P}[\mathcal{Y} \mid \phi(\mathcal{X}), f_m] \\
&= \arg \max_{v_m, \gamma_l, \gamma_r} \sum_{i=1}^n \mathbb{E}_{\mathbf{x}' \sim \phi(\mathbf{x}_i)} [\log \mathbb{P}[y_i \mid \mathbf{x}', f_m]] \\
&= \arg \max_{v_m, \gamma_l, \gamma_r} \sum_{i \in \{i|y_i=0\}} p_{l,i}(v_m) \log(1 - \gamma_l) + p_{r,i}(v_m) \log(1 - \gamma_r) \\
&\quad + \sum_{i \in \{i|y_i=1\}} p_{l,i}(v_m) \log(\gamma_l) + p_{r,i}(v_m) \log(\gamma_r)
\end{aligned}$$

$$\begin{aligned}
&= \arg \max_{v_m, \gamma_l, \gamma_r} p_l^0(v_m) \log(1 - \gamma_l) + p_r^0(v_m) \log(1 - \gamma_r) \\
&\quad + p_l^1(v_m) \log(\gamma_l) + p_r^1(v_m) \log(\gamma_r)
\end{aligned}$$

As shown in Section 4.1, for a fixed v_m , the MLE-optimal estimates for γ_l and γ_r are $\gamma_l^{\phi, \text{MLE}}(v_m) = \frac{p_l^1(v_m)}{p_l^1(v_m) + p_l^0(v_m)}$ and $\gamma_r^{\phi, \text{MLE}}(v_m) = \frac{p_r^1(v_m)}{p_r^1(v_m) + p_r^0(v_m)}$. Hence, in the following, it is enough to optimize over v_m , substituting in $\gamma_l^{\phi, \text{MLE}}(v_m)$ and $\gamma_r^{\phi, \text{MLE}}(v_m)$. We obtain:

$$\begin{aligned}
v_m^{\phi, \text{MLE}} &= \arg \max_{v_m} p_l^0(v_m) \log(1 - \gamma_l^{\phi, \text{MLE}}(v_m)) + p_r^0(v_m) \log(1 - \gamma_r^{\phi, \text{MLE}}(v_m)) \\
&\quad + p_l^1(v_m) \log(\gamma_l^{\phi, \text{MLE}}(v_m)) + p_r^1(v_m) \log(\gamma_r^{\phi, \text{MLE}}(v_m)) \\
&= \arg \max_{v_m} p_l^0(v_m) \log \left(1 - \frac{p_l^1(v_m)}{p_l^1(v_m) + p_l^0(v_m)} \right) + p_r^0(v_m) \log \left(1 - \frac{p_r^1(v_m)}{p_r^1(v_m) + p_r^0(v_m)} \right) \\
&\quad + p_l^1(v_m) \log \left(\frac{p_l^1(v_m)}{p_l^1(v_m) + p_l^0(v_m)} \right) + p_r^1(v_m) \log \left(\frac{p_r^1(v_m)}{p_r^1(v_m) + p_r^0(v_m)} \right) \\
&= \arg \max_{v_m} p_l^0(v_m) \log \left(1 - \frac{p_l^1(v_m)}{p_l(v_m)} \right) + p_r^0(v_m) \log \left(1 - \frac{p_r^1(v_m)}{p_r(v_m)} \right) \\
&\quad + p_l^1(v_m) \log \left(\frac{p_l^1(v_m)}{p_l(v_m)} \right) + p_r^1(v_m) \log \left(\frac{p_r^1(v_m)}{p_r(v_m)} \right) \\
&= \arg \max_{v_m} -H_{\text{entropy}}(v_m) \\
&= \arg \min_{v_m} H_{\text{entropy}}(v_m) \\
&= v_m^*
\end{aligned}$$

Thus, we have that the triplet $v_m^* := \arg \min_{v_m} H_{\text{entropy}}(v_m)$, $\gamma_l(v_m^*) = \frac{p_l^1(v_m^*)}{p_l^1(v_m^*) + p_l^0(v_m^*)}$ and $\gamma_r(v_m^*) = \frac{p_r^1(v_m^*)}{p_r^1(v_m^*) + p_r^0(v_m^*)}$ is jointly MLE-optimal. \square

A.3 Gradient Boosting for Certifiable Robustness

Below, we describe ROBTREEBOOST, already outlined in Section 4.2, in more detail. Formally, we aim to minimize the cross-entropy loss between the certifiable prediction at the q^{th} percentile $\mathcal{F}_{m-1, \mathbf{x}_i}^{-1}(q)$ and the one-hot target probability given by the label y , where we choose $q = \rho^{-1}(r)$ for some target radius r . Concretely, to add the m^{th} stump to our ensemble, we begin by computing the certifiable prediction y'_i :

$$y'_i = \begin{cases} \mathcal{F}_{m-1, \mathbf{x}_i}^{-1}(q) & \text{if } y = 0 \\ \mathcal{F}_{m-1, \mathbf{x}_i}^{-1}(1 - q) & \text{if } y = 1. \end{cases} \quad (5)$$

Now, we define the pseudo label \tilde{y} as the residual between the target label y and the certifiable prediction y' , scaled to $[0, 1]$ as $\tilde{y}_i = \frac{1}{2} + \frac{y_i - y'_i}{2}$. Subsequently, we select feature j_m and split position v_m that minimize the mean squared error impurity (MSE) under the randomization scheme for these pseudo-labels. As before, we define the mean squared error impurity H_{MSE} in terms of the branching probabilities $p_{l,i} = \mathbb{P}_{\mathbf{x}' \sim \phi(\mathbf{x}_i)}[x'_{j_m} \leq v_m]$ and $p_{r,i} = 1 - p_{l,i}$:

$$\mu_j = \frac{\sum_{i=1}^n p_{j,i} \tilde{y}_i}{\sum_{i=1}^n p_{j,i}} \quad H_{\text{MSE}} = \frac{\sum_{i=1}^n \sum_{j \in \{l, r\}} p_{j,i} (\tilde{y}_i - \mu_j)^2}{n}. \quad (6)$$

The optimal leaf predictions can now be computed approximately [33] to

$$\gamma_l = \frac{\sum_{i=1}^n p_{l,i} \tilde{y}_i}{\sum_i p_{l,i} |2\tilde{y}_i - 1| (1 - |2\tilde{y}_i - 1|)}, \quad (7)$$

and γ_r analogously. We initialize this boosting process with an ensemble of individually MLE-optimal stumps and repeat this boosting step until we have added as many stumps as desired.

A.4 Adaptive Boosting for Certifiable Robustness

Below, we describe ROBADA BOOST, already outlined in Section 4.2, in more detail. Our goal is to obtain a weighted ensemble \bar{F}_K

$$\bar{F}_K(\mathbf{x}) = \frac{1}{\sum_{k=1}^K \alpha^k} \sum_{k=1}^K \alpha^k \mathbb{1}_{\mathbb{P}_{\mathbf{x}' \sim \phi(\mathbf{x})}[\bar{f}_M^k(\mathbf{x}') > 0.5] > 0.5}, \quad (8)$$

consisting of K stump ensembles \bar{f}_M^k , that is certifiably robust at a pre-determined radius r . Here, $\bar{F}_K(\mathbf{x}): \mathbb{R}^d \rightarrow [0, 1]$ is a soft-classifier, that predicts class 1 for outputs > 0.5 and class 0 else.

To train the K constituting ensembles such that the overall ensemble \bar{F}_K is certifiably robust at radius r , we proceed as follows: First, we initialize the weights of all samples \mathbf{x}_i to $w_i^1 = \frac{1}{n}$. Then, for $k = 1$ to K , we iteratively fit a new stump ensemble \bar{f}_M^k as described in Section 4.1 using the sample weights w_i^k . Then, similar to Freund and Schapire [34] although targeting certifiability instead of accuracy, we update the sample weights as follows: First, we compute whether the newly trained k -th ensemble \bar{f}_M^k is certifiably correct (c_i) for each sample \mathbf{x}_i in the training set:

$$c_i = \begin{cases} \mathbb{1}_{\mathbb{P}_{\mathbf{x}' \sim \phi(\mathbf{x}_i)}[\bar{f}_M^k(\mathbf{x}') \leq 0.5] > \rho_{\mathbf{x}}^{-1}(r)} & \text{if } y = 0 \\ \mathbb{1}_{\mathbb{P}_{\mathbf{x}' \sim \phi(\mathbf{x}_i)}[\bar{f}_M^k(\mathbf{x}') > 0.5] > \rho_{\mathbf{x}}^{-1}(r)} & \text{if } y = 1. \end{cases} \quad (9)$$

Then, we determine the certifiable error err^k , and the model weight α^k of \bar{f}_M^k as:

$$err^k = \frac{\sum_{i=1}^n w_i (1 - c_i)}{\sum_{i=1}^n w_i} \quad \alpha^k = \log \frac{1 - err^k}{err^k}$$

and update the sample weights for the next iteration to:

$$w_i^{k+1} = \frac{w_i^k \exp(\alpha^k (1 - c_i))}{\sum_{i=1}^n w_i^k \exp(\alpha^k (1 - c_i))}$$

before training the next ensemble. This way, we are minimizing the overall loss for certified predictions at radius r .

To certify \bar{F}_K at a specific radius r , we now have to show that we can certify individual ensembles corresponding to at least half the total weights, or more formally (here, without loss of generality assuming a label of $y = 1$):

$$\sum_{k=1}^K \alpha^k \mathbb{1}_{\mathbb{P}_{\mathbf{x}' \sim \phi(\mathbf{x})}[\bar{f}_M^k(\mathbf{x}') > 0.5] > \rho_{\mathbf{x}}^{-1}(r)} > \frac{\sum_{k=1}^K |\alpha^k|}{2}. \quad (10)$$

To compute the certifiable radius for \bar{F}_K , we compute the certifiable radii R^k of the individual ensembles, sort them in decreasing order such that $R^k \geq R^{k+1}$ and obtain the largest radius R^k such that $\sum_{l=1}^k \alpha^l > \frac{\sum_{l=1}^K |\alpha^l|}{2}$. Intuitively, we need to find a subset of models such that their weighted predictions for class 1 reach at least half the possible weight, accounting for negative weights.

B Experimental Details

Here, we describe our experimental setup in greater detail. Note that we also publish all code, models, and instructions required to reproduce our results at ANONYMIZED.

B.1 Datasets

In this section, we describe the datasets we use in detail.

Datasets with Numerical Features We conduct our experiments considering exclusively numerical features on the same datasets as prior work [23, 22]. More concretely, we use the tabular datasets BREASTCANCER [37] and DIABETES [36], where we follow prior work [23] in using the first 80% of the samples as train set and the remaining 20% as test set, normalizing the data to $[0, 1]$, and the

vision datasets MNIST 1 vs. 5 [39], MNIST 2 vs. 6 [39], and FMNIST-SHOES [38], where we use all samples of the right classes from the train and test sets.

Datasets with Numerical and Categorical Features We conduct our experiments on the joint certification of numerical and categorical features using the popular ADULT [37] and CREDIT [37] datasets. For both, we use the first 70% of the samples as the train set, and the remaining 30% as the test set. Here, we normalize the numerical features using the mean and standard deviation of the training data, before applying any perturbations.

The ADULT [37] dataset is a societal dataset based on the 1994 US Census database. It contains eight categorical and six numerical variables for each individual. The cardinalities of the categorical variables range from 2 to 42 (concretely, they are 9, 16, 7, 15, 6, 5, 2, and 42). The task is to predict whether an individual’s salary is below or above 50k USD.

The CREDIT [37] dataset is a financial dataset containing 13 categorical and 7 numerical features. The cardinalities of the categorical features range from 2 to 10 (concretely, they are 4, 5, 10, 5, 5, 4, 3, 4, 3, 3, 4, 2, and 2). The task is to predict whether a customer has a low or high risk to default on a loan.

Both datasets exhibit a significant class imbalance, with the minority class constituting 24.6% of the ADULT and 29.6% of the CREDIT train set. Therefore, we report balanced certified accuracy, computed as the arithmetic mean of the per class certified accuracies.

B.2 Training Details

The key (and for independent training, the only) hyper-parameter of our approach is the noise magnitude, λ for ℓ_1 -certification and σ for ℓ_2 -certification. In Table 5, we report the noise levels chosen for the different datasets. We discuss the effect of different noise magnitudes in App. C.4 and observe that results are generally quite stable across a wide range of noise magnitudes. Unless otherwise stated, we determine the split position v_m via linear search using increments of size 0.01 and discretize leaf predictions γ using 100 steps (i.e., $\Delta = 100$).

ROBTREEBOOST We initialize ROBTREEBOOST with an ensemble of independently trained stumps and add a further n_b stumps as described in Section 4.2 using the q^{th} percentile to compute the certifiable predictions. We chose q and n_b as shown in Table 6.

ROBADABOOST To evaluate ROBADABOOST, we consider ensembles of $K = 20$ individual stump ensembles in each of our experiments. We choose the same noise magnitudes as for independently trained stumps, described in Table 5.

Joint Certification For joint certification, we use ensembles of independently trained decision stumps, one for each feature. The stump corresponding to categorical features maps a categorical value to either 0.375 or 0.625 (which are the same distance from the decision threshold 0.5), depending on whether the majority of the samples with this categorical value have class 0 or 1, respectively. Note that permitting arbitrary leaf predictions slightly improves clean accuracy, but significantly worsens worst-case behaviour. Choosing leaf predictions further from the decision threshold gives more emphasis to categorical variables compared to numerical ones. The stumps for the numerical features are learned individually, as described in Section 4.1. For ℓ_1 , we used the noise magnitude $\lambda = 2.0$ and for ℓ_2 -certification $\sigma = 0.25$.

Table 5: Noise levels λ for ℓ_1 and σ for ℓ_2 -certification utilized for Table 2 for various datasets.

Method	Dataset	λ (for ℓ_1)	σ (for ℓ_2)
Independent	BREASTCANCER	2.00	4.00
	DIABETES	0.35	0.25
	MNIST 1 vs. 5	4.00	0.25
	MNIST 2 vs. 6	4.00	0.25
	FMNIST-SHOES	4.00	0.25
Boosting	BREASTCANCER	2.00	0.25
	DIABETES	0.28	0.15
	MNIST 1 vs. 5	4.00	0.25
	MNIST 2 vs. 6	4.00	0.25
	FMNIST-SHOES	4.00	0.25

Table 6: ROBTREEBOOST parameters.

Parameter	Perturbation	BREASTCANCER	DIABETES
Percentile q	ℓ_1	0.60	0.70
	ℓ_2	0.98	0.95
Additional stumps n_b	ℓ_1	30	15
	ℓ_2	40	100

Table 8: Certified accuracy (CA) [%] under joint ℓ_0 - and ℓ_2 -perturbations of categorical and numerical features, respectively, depending on whether model uses categorical and/or numerical features. The natural accuracy is the CA at radius $r = 0.0$. Larger is better.

Dataset	Categorical Features	ℓ_0 Radius r_0	CA without Numerical Features	CA with Numerical Features at ℓ_2 Radius r_2						
				0.00	0.25	0.50	0.75	1.00	1.25	1.50
ADULT	no	-	-	74.4	65.6	37.3	23.7	10.4	5.1	2.5
		0	70.2	69.7	65.5	58.7	54.4	35.4	25.7	20.3
	yes	1	52.4	57.6	53.3	44.7	38.1	22.3	14.4	11.0
		2	27.8	43.4	38.8	29.1	20.5	12.1	8.8	6.6
		3	6.7	29.6	24.8	17.2	9.0	5.1	4.0	2.8
CREDIT	no	-	-	55.0	44.7	30.0	16.7	9.3	6.7	4.0
		0	71.0	73.7	69.7	66.3	60.7	58.3	55.7	53.7
	yes	1	49.3	52.3	48.7	42.0	39.0	37.3	35.7	34.3
		2	26.7	31.0	27.7	24.7	20.3	17.0	13.7	13.0
		3	8.7	14.3	11.3	8.7	6.3	5.7	5.0	4.3

B.3 Computational Resources and Experimental Timings

In this section, we describe the computational resources required for our experiments. We run all our experiments using 24 cores of an Intel Xeon Gold 6242 CPUs and a single NVIDIA RTX 2080Ti and report timings for the full experiment in App. B.3. We show timings in Table 7.

We observe that all certification is extremely quick with FMNIST-SHOES taking the longest at 6s for the whole test set and an ensemble of independently trained stumps in the ℓ_1 -setting, translating to 0.003s per sample. When evaluating models in single instead of double precision, we can, e.g., further reduce certification times from 3s to 1.2s for MNIST 2 vs. 6. The independently MLE-optimal training is similarly quick, allowing us to run all core experiments in less than 5 minutes. Only ROBADA BOOST takes more than one minute for an individual experiment, as it involves training and certifying 20 stump ensembles. For datasets combining categorical and numerical features, the training and certification for the categorical variables is almost instantaneous and dominated by that for the numerical features. The latter requires 19.9s and 47.0s for the ℓ_1 and ℓ_2 -experiment, respectively, on ADULT and 1.5s respectively 2.0s on CREDIT. We remark that computational efficiency was not a main focus of this work and we did not optimize runtimes.

Table 7: Experimental timings for whole datasets.

Norm	Dataset	Independent		Boosting	
		Training	Certification	Training	Certification
ℓ_1	BREASTCANCER	2s	< 0.1s	14s	< 0.1s
	DIABETES	2s	< 0.1s	2s	< 0.1s
	MNIST 1 vs. 5	32s	5s	13min	27s
	MNIST 2 vs. 6	29s	4s	11min	16s
	FMNIST-SHOES	31s	6s	13min	40s
ℓ_2	BREASTCANCER	2s	< 0.1s	9s	< 0.1s
	DIABETES	2s	< 0.1s	47s	< 0.1s
	MNIST 1 vs. 5	14s	4s	10min	29s
	MNIST 2 vs. 6	14s	3s	9min	26s
	FMNIST-SHOES	15s	4s	9min	27s

C Additional Experiments

In this section, we extend our experimental evaluation from Section 5. Concretely, in App. C.1, we provide additional experiments on the joint certification of categorical and numerical variables. In App. C.2, we compare DRS to RS in more detail while in App. C.3, we continue our investigation of our MLE optimality criterion. Moreover, in App. C.4, we provide additional experiments on the effect of the noise magnitudes λ and σ for ℓ_1 - and ℓ_2 -certification, respectively. Finally, in App. C.5, we analyze the impact of the discretization granularity and in App. C.6, we evaluate the effect of an approximate split position optimization.

C.1 Additional Experiments on Joint Robustness Certificates

In Table 8, we report the (unbalanced) certified accuracies corresponding to the balanced ones reported in Table 3.

Similarly, we report the balanced and unbalanced certified accuracies at a range of ℓ_1 radii over the numerical features given varying perturbations of the categorical features in Tables 9 and 10 and observe similar trends as in the ℓ_2 -setting. In particular, models utilizing both categorical and numerical features outperform those using only either one on clean data. Interestingly, the slower drop

Table 9: Balanced certified accuracy (BCA) [%] under joint ℓ_0 - and ℓ_1 -perturbations of categorical and numerical features, respectively, depending on whether model uses categorical and/or numerical features. The balanced natural accuracy is the BCA at radius $r = 0.0$. Larger is better.

Dataset	Categorical Features	ℓ_0 Radius r_0	BCA without Numerical Features	BCA with Numerical Features at ℓ_1 Radius r_1						
				0.00	0.25	0.50	0.75	1.00	1.25	1.50
ADULT	no	-	-	62.8	59.4	54.9	51.7	47.7	44.8	42.3
		0	76.6	77.3	76.7	76.0	75.4	74.3	73.1	71.7
	yes	1	57.4	60.1	59.5	58.7	57.9	57.1	56.3	55.2
		2	33.5	39.0	37.9	37.0	36.2	35.6	35.1	34.4
		3	8.9	17.6	15.8	14.7	13.7	12.8	12.2	11.8
CREDIT	no	-	-	58.4	56.1	52.0	50.4	39.5	32.6	25.1
		0	70.7	71.2	71.2	71.2	71.2	71.0	71.0	70.2
	yes	1	48.2	49.0	48.8	48.0	48.0	46.8	46.1	45.5
		2	26.4	28.0	27.8	27.6	26.5	26.5	26.5	24.9
		3	7.8	8.0	8.0	8.0	7.8	7.8	7.8	6.8

Table 10: Certified accuracy (CA) [%] under joint ℓ_0 - and ℓ_1 -perturbations of categorical and numerical features, respectively, depending on whether model uses categorical and/or numerical features. The natural accuracy is the CA at radius $r = 0.0$. Larger is better.

Dataset	Categorical Features	ℓ_0 Radius r_0	CA without Numerical Features	CA with Numerical Features at ℓ_1 Radius r_1						
				0.00	0.25	0.50	0.75	1.00	1.25	1.50
ADULT	no	-	-	80.0	77.3	72.8	69.4	64.5	61.1	58.0
		0	70.2	70.3	69.7	68.8	67.9	66.5	65.2	63.9
	yes	1	52.4	53.9	53.3	52.6	51.8	50.9	50.1	49.1
		2	27.8	32.4	31.3	30.3	29.3	28.7	28.3	27.8
		3	6.7	12.5	11.3	10.3	9.4	8.7	8.3	8.1
CREDIT	no	-	-	68.3	66.0	60.7	59.3	46.3	39.3	31.3
		0	71.0	71.3	71.3	71.3	71.3	71.0	71.0	70.3
	yes	1	49.3	49.7	49.3	48.7	48.7	47.0	46.0	45.7
		2	26.7	27.7	27.3	27.0	26.3	26.3	26.3	25.0
		3	8.7	9.0	9.0	9.0	8.7	8.7	8.7	7.3

in certified accuracy with increasing perturbation of the numerical features is much more pronounced in the ℓ_1 -setting, and much higher certified accuracies are obtained even at large radii. For example, on ADULT, just considering numerical features leads to a BCA of 62.8% at radius $r_1 = 0.0$ dropping to 42.3% at $r_1 = 1.5$. In contrast, when also utilizing categorical features, the BCA at $r_1 = 0.0$ is 77.3% dropping only to 71.7% at $r_1 = 1.5$, when no categorical variable is perturbed ($r_0 = 0$). Similarly, when at most one categorical variable is perturbed, the BCA at $r_1 = 0.0$ is 60.1% and drops only to 55.2% radius $r_1 = 1.5$. This highlights that, when available, utilizing categorical features in addition to the numerical ones is essential and can make models significantly more certifiably robust to perturbations of the numerical variables, even when categorical variables can be perturbed as well.

C.2 Derandomized vs. Randomized Smoothing

Here, we compare evaluating stump ensembles deterministically via DRS (Section 3) to sampling-based RS [24]. In Table 11, we provide quantitative results corresponding to Fig. 6, expanded by an equivalent experiment for ℓ_1 -norm perturbations. We observe that as sampling-based RS uses increasingly more samples, it converges towards DRS. This convergence is much faster in the ℓ_1 -setting. However, especially in the ℓ_2 -setting, a notable gap remains even when using as many as 100 000 samples. This is expected as sampling-based RS computes a lower confidence bound to the true success probability, which can be computed exactly with DRS. Thus the higher the desired confidence, the larger this gap will be. Further, if RS were to yield a larger radius than DRS, this would actually be an error, occurring with probability α , as DRS computes the true maximum certifiable radius. This highlights another key difference: RS provides probabilistic guarantees that hold with confidence $1 - \alpha$, while DRS provides deterministic guarantees. Moreover, for RS, many samples have to be evaluated (typically $n = 100\,000$), while DRS can efficiently compute the exact CDF. We note that the much larger improvement in certified radii observed for ℓ_2 -norm perturbations

Table 11: We compare certifying the same stump ensembles via Deterministic Smoothing (DRS) and Randomized Smoothing (RS) with respect to the average certified radius (ACR) and the certified accuracy [%] at numerous radii r on MNIST 1 vs. 5 for ℓ_1 ($\lambda = 4.0$) and ℓ_2 ($\sigma = 0.5$) norm perturbations. Larger is better.

Norm	Method	ACR	Certified Accuracy at Radius r							
			0.0	0.50	1.00	1.50	2.00	2.50	3.00	3.50
ℓ_1	RS ($n = 100$)	2.809	93.0	91.2	88.6	86.2	82.9	77.0	68.8	0.0
	RS ($n = 1000$)	3.337	95.6	94.4	92.8	90.6	87.8	84.7	79.5	70.4
	RS ($n = 10000$)	3.430	96.0	95.3	93.7	91.6	89.4	85.8	82.1	73.8
	RS ($n = 100000$)	3.456	96.1	95.5	94.0	91.9	89.9	86.3	82.9	74.6
	DRS (ours)	3.467	96.6	95.6	94.1	92.1	89.9	86.5	83.1	75.1
ℓ_2	RS ($n = 100$)	0.680	94.8	90.1	0.0	0.0	0.0	0.0	0.0	0.0
	RS ($n = 1000$)	1.102	95.6	92.5	85.0	0.0	0.0	0.0	0.0	0.0
	RS ($n = 10000$)	1.403	95.9	92.9	86.9	75.0	0.0	0.0	0.0	0.0
	RS ($n = 100000$)	1.627	95.9	93.0	87.3	78.1	0.0	0.0	0.0	0.0
	DRS (ours)	2.161	96.0	93.0	87.5	79.0	65.3	40.5	12.3	5.9

Table 12: We compare training stump ensembles optimally via MLE-optimal criterion, training them via noisy sampling (Sampling) and default training (Default) with respect to the average certified radius (ACR) and the certified accuracy [%] on MNIST 2 vs. 6 at numerous radii r on various norms for multiple noise magnitudes (λ for ℓ_1 and σ for ℓ_2). Larger is better.

Norm	λ (ℓ_1) or σ (ℓ_2)	Method	ACR	Certified Accuracy at Radius r							
				0.0	0.5	1.0	1.5	2.0	2.5	3.0	3.5
ℓ_1	1.0	Default	0.519	51.9	51.9	51.9	0.0	0.0	0.0	0.0	0.0
		Sampling	0.928	96.2	93.9	64.8	0.0	0.0	0.0	0.0	0.0
		MLE (Ours)	0.931	96.2	94.3	66.2	0.0	0.0	0.0	0.0	0.0
	4.0	Default	2.074	51.9	51.9	51.9	51.9	51.9	51.9	51.9	51.9
		Sampling	3.166	96.3	95.0	93.3	90.5	87.3	81.4	72.5	56.0
		MLE (Ours)	3.282	96.3	95.4	93.9	91.7	88.7	84.1	76.0	62.8
	16.0	Default	8.297	51.9	51.9	51.9	51.9	51.9	51.9	51.9	51.9
		Sampling	6.646	96.4	95.3	94.4	93.4	91.8	90.0	87.8	84.9
		MLE (Ours)	8.574	96.2	95.7	95.0	94.1	93.2	91.7	90.6	88.4
ℓ_2	0.25	Default	0.967	51.9	51.9	51.8	48.7	0.0	0.0	0.0	0.0
		Sampling	1.628	96.3	92.8	85.9	71.7	0.0	0.0	0.0	0.0
		MLE (Ours)	1.642	96.3	93.0	86.3	73.0	0.0	0.0	0.0	0.0
	1.0	Default	3.436	51.9	51.9	51.9	51.9	51.9	51.9	51.9	51.9
		Sampling	1.594	95.5	89.1	76.5	57.9	33.5	11.7	2.1	0.2
		MLE (Ours)	1.724	95.5	90.1	79.2	62.5	40.3	18.7	5.4	1.3
	4.0	Default	12.167	51.9	51.9	51.9	51.9	51.9	51.9	51.9	51.9
		Sampling	1.095	89.2	72.9	50.9	32.6	15.8	4.0	0.5	0.0
		MLE (Ours)	1.652	95.1	88.7	76.5	59.2	36.6	16.3	4.9	1.5

is due to the significantly higher sensitivity of the certifiably radius w.r.t. the success probability (see Table 1).

C.3 MLE Optimality Criterion

In Table 12, we compare our robust MLE optimality criterion (MLE) to applying the standard entropy criterion to samples drawn from the input randomization scheme (Sampling) or the clean data (Default). We observe that training approaches accounting for randomness (i.e., Sampling and MLE) consistently outperform default training. In some cases, default training even suffers from a mode collapse, always predicting the same class. Amongst the two methods accounting for the input randomization, our MLE optimality criterion consistently outperforms samplings at all noise magnitudes and for both perturbation types. This effect is particularly pronounced at large noise magnitudes, where sampling becomes less effective at capturing the input distribution.

Table 13: Comparison of average certified radius (ACR) and certified accuracy at various radii r with respect to the ℓ_1 norm for numerous datasets and noise magnitudes λ . Larger is better.

Dataset	λ	ACR	Certified Accuracy at Radius r										
			0.0	1.0	2.0	3.0	4.0	5.0	6.0	7.0	8.0	9.0	10.0
FMNIST-SHOES	0.5	0.407	84.4	0.0	0.0	0.0	0.0	0.0	0.0	0.0	0.0	0.0	0.0
	1.0	0.766	83.5	55.1	0.0	0.0	0.0	0.0	0.0	0.0	0.0	0.0	0.0
	2.0	1.463	83.7	74.9	47.0	0.0	0.0	0.0	0.0	0.0	0.0	0.0	0.0
	4.0	2.780	85.8	80.2	73.3	60.9	21.3	0.0	0.0	0.0	0.0	0.0	0.0
	8.0	4.755	83.9	80.0	75.5	70.3	63.9	56.4	46.5	32.6	1.9	0.0	0.0
	16.0	7.975	84.3	81.7	77.8	75.0	71.7	67.3	63.2	57.9	52.9	47.0	41.1
MNIST 1 vs. 5	0.5	0.476	96.3	0.0	0.0	0.0	0.0	0.0	0.0	0.0	0.0	0.0	0.0
	1.0	0.934	96.3	77.0	0.0	0.0	0.0	0.0	0.0	0.0	0.0	0.0	0.0
	2.0	1.808	96.2	92.1	62.8	0.0	0.0	0.0	0.0	0.0	0.0	0.0	0.0
	4.0	3.467	96.6	94.1	89.9	83.1	39.1	0.0	0.0	0.0	0.0	0.0	0.0
	8.0	6.472	97.0	95.4	93.3	91.0	87.4	82.2	75.1	60.7	4.4	0.0	0.0
	16.0	8.957	90.4	88.6	86.6	83.5	80.3	77.4	72.9	67.4	61.9	56.2	49.6
MNIST 2 vs. 6	0.5	0.477	96.3	0.0	0.0	0.0	0.0	0.0	0.0	0.0	0.0	0.0	0.0
	1.0	0.931	96.2	66.2	0.0	0.0	0.0	0.0	0.0	0.0	0.0	0.0	0.0
	2.0	1.780	96.2	92.2	43.0	0.0	0.0	0.0	0.0	0.0	0.0	0.0	0.0
	4.0	3.282	96.3	93.9	88.7	76.0	3.8	0.0	0.0	0.0	0.0	0.0	0.0
	8.0	5.617	96.5	94.6	91.4	87.4	80.9	71.7	56.6	31.3	0.0	0.0	0.0
	16.0	8.574	96.2	95.0	93.2	90.6	86.5	82.7	77.5	70.5	62.7	53.3	41.3

Table 14: Comparison of average certified radius (ACR) and certified accuracy at various radii r with respect to the ℓ_2 norm for numerous datasets and noise magnitudes σ . Larger is better.

Dataset	σ	ACR	Certified Accuracy at Radius r							
			0.0	0.5	1.0	1.5	2.0	2.5	3.0	3.5
FMNIST-SHOES	0.25	1.361	86.8	79.6	70.0	58.2	0.0	0.0	0.0	0.0
	0.5	1.723	86.5	78.9	70.1	56.6	42.2	27.8	17.4	8.4
	1.0	1.699	86.2	78.5	69.1	55.7	41.0	25.8	16.9	8.9
	2.0	1.681	86.2	78.5	68.8	55.1	40.2	25.6	16.8	8.7
	4.0	2.136	57.1	52.2	49.7	47.9	46.0	43.4	39.4	35.0
	8.0	1.518	83.7	74.2	64.4	51.0	35.4	21.0	10.4	4.8
MNIST 1 vs. 5	0.25	1.737	95.8	93.6	89.0	82.8	0.0	0.0	0.0	0.0
	0.5	2.161	96.0	93.0	87.5	79.0	65.3	40.5	12.3	5.9
	1.0	2.044	96.0	92.7	86.1	75.6	57.3	28.4	11.4	6.7
	2.0	2.012	95.8	92.7	85.8	74.9	56.2	26.9	10.3	6.0
	4.0	1.875	94.8	87.2	71.8	48.1	34.7	29.9	23.8	15.7
	8.0	1.808	96.1	90.2	80.3	62.9	36.4	20.4	13.3	7.7
MNIST 2 vs. 6	0.25	1.642	96.3	93.0	86.3	73.0	0.0	0.0	0.0	0.0
	0.5	1.824	95.8	91.2	81.9	66.7	46.4	23.4	7.4	1.3
	1.0	1.724	95.5	90.1	79.2	62.5	40.3	18.7	5.4	1.3
	2.0	1.688	95.4	89.5	78.0	60.9	38.8	17.5	4.9	1.0
	4.0	1.652	95.1	88.7	76.5	59.2	36.6	16.3	4.9	1.5
	8.0	1.718	74.3	61.0	53.2	49.4	46.6	40.2	30.3	17.4

C.4 Effect of Noise Level

Here, we provide additional experiments for varying noise magnitudes, λ for ℓ_1 -certification, and σ for ℓ_2 -certification. In Tables 13 and 14, we provide extensive experiments for the ℓ_1 - and ℓ_2 -setting, respectively, which we visualize in Figs. 7 and 8.

We observe that, in the ℓ_1 -setting, the natural accuracy (certified accuracy at radius 0) is quite insensitive to an increase in noise magnitude. Consequently, large λ lead to exceptionally large ACR and certified accuracies even at large radii, e.g., on MNIST 2 vs. 6, we obtain a certified accuracy of 82.7% at ℓ_1 -radius $r = 5.0$.

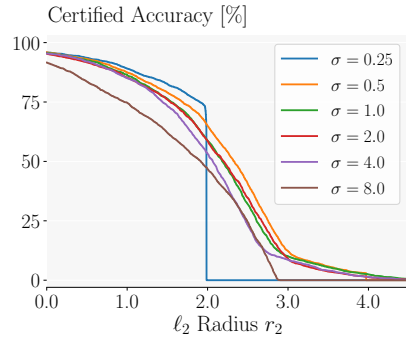


Figure 8: Comparing DRS for various noise levels σ on MNIST 1 vs. 5.

Table 15: We compare the performance of models for different number of discretization sizes with respect to average certified radius (ACR) and given certified accuracies (CA) [%] on MNIST 1 vs. 5. We utilize $\lambda = 4.0$ for ℓ_1 and $\sigma = 0.5$ for ℓ_2 . Larger is better.

Norm	Discretizations	ACR	Certified Accuracy [%] at Radius r							
			0.00	0.50	1.00	1.50	2.00	2.50	3.00	3.50
ℓ_1	2	1.834	59.1	51.6	45.1	44.0	44.0	44.0	44.0	43.9
	3	2.240	56.0	56.0	56.0	56.0	56.0	56.0	56.0	56.0
	5	2.240	56.0	56.0	56.0	56.0	56.0	56.0	56.0	56.0
	10	2.167	71.4	67.4	63.1	58.0	53.4	48.1	44.6	43.9
	25	2.240	56.0	56.0	56.0	56.0	56.0	56.0	56.0	56.0
	50	3.530	96.9	96.1	94.8	93.4	91.6	89.0	85.2	78.5
	100	3.467	96.6	95.6	94.1	92.1	89.9	86.5	83.1	75.1
	250	3.432	96.1	94.9	93.5	91.5	88.9	85.6	81.5	73.9
	500	3.421	95.9	94.8	93.2	91.5	88.6	85.5	81.0	73.5
	1000	3.413	95.8	94.6	93.0	91.5	88.4	85.2	80.5	73.3
ℓ_2	2	1.747	44.0	44.0	44.0	44.0	44.0	44.0	44.0	44.0
	3	2.223	56.0	56.0	56.0	56.0	56.0	56.0	56.0	56.0
	5	2.223	56.0	56.0	56.0	56.0	56.0	56.0	56.0	56.0
	10	2.076	96.6	92.6	87.3	77.2	57.5	27.8	15.3	9.1
	25	2.371	88.5	84.0	77.1	69.6	62.5	55.0	46.4	30.9
	50	2.152	96.2	93.0	87.7	78.9	64.3	39.1	12.0	6.4
	100	2.161	96.0	93.0	87.5	79.0	65.3	40.5	12.3	5.9
	250	2.165	95.9	93.1	87.5	79.1	65.4	41.5	12.5	5.8
	500	2.168	95.8	93.1	87.3	79.1	65.6	42.0	12.4	5.6
	1000	2.168	95.8	93.1	87.3	79.1	65.7	42.0	12.4	5.6

In the ℓ_2 -setting, increasing the noise magnitude σ generally leads to a more pronounced drop in natural and certified accuracy, and thus similar ACRs for various noise magnitudes.

Thinking Outside the Box Analysing this surprising behaviour in the ℓ_1 -setting, we empirically find that despite the data being normalized to $[0, 1]$, the MLE optimality criterion often yields split positions v_m outside of $[0, 1]$. Recall that there, uniformly distributed random noise is added to the original sample ($x' \sim \text{Unif}([x - \lambda, x + \lambda]^d)$). In Fig. 9, we show a histogram of the split positions (v_m), illustrating this behaviour. In the ℓ_1 -setting and using $\lambda = 2$, all split positions are either smaller than -1 or larger than 1.9 , which are exactly the borders of uniform distributions with $\lambda = 2$ centered at the extremes of the image domain ($[0, 1]$). As all splits are outside the hyperbox constituting the original image domain, we refer to this behaviour as ‘thinking outside the box’. Intuitively, each unperturbed data point is on the same side of v_m in this case, but when the randomization scheme is applied, a split outside of $[-1, 2]$ leads to a probability mass of 0 for an original feature value of 0 or 1, while for the other, the probability mass can be as high as $\frac{1}{2\lambda}$. Therefore, such splits allow the smoothed model to still separate these cases well for randomized inputs.

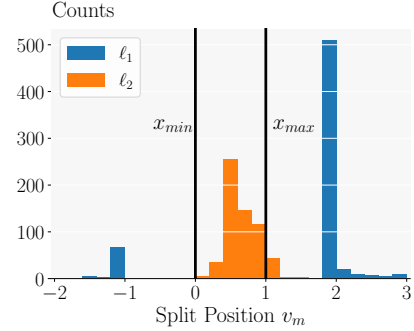


Figure 9: Comparing counts for values of v_m on MNIST 2 vs. 6 for ℓ_1 and ℓ_2 norms with $\lambda = 2.0$ and $\sigma = 0.25$, respectively.

While we observe this effect on all datasets in the ℓ_1 -setting given a sufficiently large λ , it does not appear in the ℓ_2 -setting. There, v_m ’s are typically clustered closely around or inside $[0, 1]$, as the Gaussian randomization applied here has unbounded support and does not permit for such a clean separation, regardless of the choice of v_m .

C.5 Leaf Prediction Discretization

In the main paper, all experiments are conducted with leaf predictions discretized to $\Delta = 100$ values to enable our efficient CDF computation. In this section, we investigate the effect of this discretization. Concretely, we report results on MNIST 1 vs. 5 using a range of discretization-granularities from 2 to 1000 in Table 15. While using a very coarse discretization can lead to a mode collapse and generally degraded performance, we observe that once we use at least 50 values, a finer discretization

Table 16: We compare the performance of models for different binning sizes with respect to average certified radius (ACR) and given certified accuracies (CA) [%] on MNIST 1 vs. 5. We utilize $\lambda = 4.0$ for ℓ_1 and $\sigma = 0.5$ for ℓ_2 . Larger is better.

Norm	Binning Size	ACR	Certified Accuracy [%] at Radius r							
			0.00	0.50	1.00	1.50	2.00	2.50	3.00	3.50
ℓ_1	4.0	3.452	96.2	95.2	93.6	91.7	89.4	86.3	82.7	75.3
	2.0	3.452	96.2	95.2	93.6	91.7	89.4	86.3	82.7	75.3
	1.0	3.468	96.5	95.6	94.1	92.0	89.9	86.5	83.1	75.2
	0.5	3.465	96.6	95.5	94.2	91.9	89.9	86.6	83.1	75.0
	0.1	3.462	96.6	95.5	94.2	92.0	89.9	86.4	83.0	74.8
	0.05	3.466	96.5	95.6	94.1	91.9	89.9	86.5	83.1	75.1
	0.01	3.467	96.6	95.6	94.1	92.1	89.9	86.5	83.1	75.1
	0.005	3.467	96.6	95.6	94.1	92.1	89.9	86.5	83.1	75.1
	0.001	3.467	96.5	95.6	94.1	92.1	90.0	86.5	83.1	75.1
	0.0005	3.466	96.5	95.5	94.1	92.1	90.0	86.5	83.0	75.1
	0.0001	3.467	96.5	95.5	94.2	92.1	89.9	86.5	83.1	75.1
ℓ_2	4.0	0.584	56.0	55.9	31.5	0.0	0.0	0.0	0.0	0.0
	2.0	1.888	95.4	91.3	83.6	73.9	55.7	22.4	4.0	0.8
	1.0	1.980	95.7	92.0	84.1	74.0	58.8	35.2	4.8	0.6
	0.5	2.119	95.8	93.0	87.2	78.5	62.6	35.7	11.5	6.5
	0.1	2.161	96.0	93.1	87.5	79.1	65.2	40.8	12.3	5.9
	0.05	2.160	96.0	93.1	87.5	79.1	65.3	41.4	12.4	5.8
	0.01	2.161	96.0	93.0	87.5	79.0	65.3	40.5	12.3	5.9
	0.005	2.163	96.0	93.1	87.5	79.0	65.3	40.9	12.4	5.9
	0.001	2.164	96.0	93.0	87.5	79.0	65.3	41.1	12.5	5.8
	0.0005	2.164	96.0	93.0	87.5	79.0	65.3	41.2	12.5	5.8
	0.0001	2.163	96.0	93.0	87.5	79.0	65.3	41.1	12.5	5.8

has only a minimal effect on the model behaviour. This suggests, that using $\Delta = 100$ our discretized smoothed model behaves very similar to a non-discretized one.

C.6 Split Position Search Granularity

In our main paper, all experiments are conducted using a step size of 0.01 to conduct the line search for the optimal split position v_m . In Table 16, we report results for search granularities from 4.0 to 10^{-4} and observe that a step size of 0.1 is sufficiently fine and reducing it further does not improve the performance of the obtained models. This suggest that our approximate optimization based on line search comes very close to the finding the true optimal split position and thus jointly MLE optimal v_m and γ .